NOAA Technical Report NESDIS 28

DUPLICATE
WITHDRAWN

The AVHRR/HIRS Operational Method for Satellite Based Sea Surface Temperature Determination

Washington, DC
March 1987

U.S. DEPARTMENT OF COMMERCE

National Oceanic and Atmospheric Administration

National Environmental Satellite, Data, and Information Service

NOAA TECHNICAL REPORTS

National Environmental Satellite, Data, and Information Service

The National Environmental Satellite, Data, and Information Service (NESDIS) manages the Nation's civil operational Earth-observing satellite systems, as well as global national data bases for meteorology, oceanography, geophysics, and solar-terrestrial sciences. From these sources, it develops and disseminates environmental data and information products critical to the protection of life and property, national defense, the national economy, energy development and distribution, global food supplies, and the development of natural resources.

Publication in the NOAA Technical Report series does not preclude later publication in scientific journals in expanded or modified form. The NESDIS series of NOAA Technical Reports is a continuation of the former NESS and EDIS series of NOAA Technical Reports and the NESC and EDS series of Environmental Science Services Administration (ESSA) Technical Reports.

These reports are available from the National Technical Information Service (NTIS), U.S. Department of Commerce, Sills Bldg., 5285 Port Royal Road, Springfield, VA 22161. Prices on request for paper copies or microfiche.

A more complete listing of these reports, by title and NTIS accession number, is available from the Assessment and Information Services Center, National Oceanic and Atmospheric Administration, Code E/AI13, Page Bldg. 2, 3300 Whitehaven Street, N.W., Washington, DC 20235. A partial listing of more recent reports appears below:

NESS Series

NESS 89 A Statistical Approach to Rainfall Estimation Using Satellite and Conventional Data. Linwood F. Whitney, Jr. April 1982. (PB82 215435)

NESS 90 Total Precipitable Water and Rainfall Determinations From the SEASAT Scanning Multichannel Microwave Radiometer (SMMR). John C. Alishouse, May 1982. (PB83 138263)

NESS 91 Numerical Smoothing and Differentiation by Finite Differences. Henry E. Fleming and Lawrence J. Crone, May 1982. (PB82-258385)

NESS 92 Satellite Infrared Observations of Oceanic Long Waves in the Eastern Equatorial Pacific 1975 to 1981. Richard Legeckis, November 1982. (PB83 161133)

NESS 93 A Method for Improving the Estimation of Conditional Instability from Satellite Retrievals. W.E. Togstad, J.M. Lewis, and H.M. Woolf, November 1982. (PB83 169938)

EDIS Series

EDS 29 GATE Convection Subprogram Data Center: Final Report on Rawinsonde Data Validation. Robert W. Reeves, March 1978. (PB-281-861)

EDS 30 Gamma Distribution Bias and Confidence Limits. Harold L. Crutcher and Raymond L. Joiner, September 1978. (PB-289-721)

EDIS 31 Calibration and Intercomparison of the GATE C-Band Radars. M. Hudlow, R. Arkell, V. Patterson, P. Pytlowany, F. Richards, and S. Geotis (MIT), November 1979. (PB81 120305)

EDIS 32 Distribution of Radiosonde Errors. Harold L. Crutcher, May 1979. (PB-297-383)

EDIS 33 Accurate Least-Squares Techniques Using the Orthogonal Function Approach. Jerry Sullivan, March 1980. (PB80 223241)

EDIS 34 An Application of Stochastic Forecasting to Monthly Averaged 700 mb Heights. Albert Koscielny, June 1982. (PB82 244625)

NESDIS Series

NESDIS 1 Satellite Observations on Variations in Southern Hemisphere Snow Cover. Kenneth F. Dewey and Richard Heim, Jr., June 1983. (PB83 252908)

NESDIS 2 NODC 1 An Environmental Guide to Ocean Thermal Energy Conversion (OTEC) Operations in the Gulf of Mexico. National Oceanographic Data Center (DOC/NOAA Interagency Agreement Number EX-76-A-29-1041), June 1983. (PB84 115146)

NESDIS 3 Determination of the Planetary Radiation Budget From TIROS-N Satellites. Arnold Gruber, Irwin Ruff, and Charles Earnest, August 1983. (PB84 100916)

NESDIS 4 Some Applications of Satellite Radiation Observations to Climate Studies. T. S. Chen, George Ohring, and Haim Ganot, September 1983. (PB84 108109)

NESDIS 5 A Statistical Technique for Forecasting Severe Weather From Vertical Soundings by Satellite and Radiosonde. David L. Keller and William L. Smith, June 1983. (PB84 114099)

(Continued on inside back cover)

NOAA Technical Report NESDIS 28

The AVHRR/HIRS Operational Method for Satellite Based Sea Surface Temperature Determination

Charles Walton

Washington, DC
March 1987

U.S. DEPARTMENT OF COMMERCE
Malcolm Baldrige, Secretary

National Oceanic and Atmospheric Administration
Anthony J. Calio, Under Secretary

National Environmental Satellite, Data, and Information Service
Thomas N. Pyke, Assistant Administrator

TABLE OF CONTENTS

The AVHRR/HIRS Operational Method for Satellite Based Sea Surface Temperature Determination

Charles Walton

National Environmental Satellite, Data and Information Service
National Oceanic and Atmospheric Administration

Washington, D.C. 20233

ABSTRACT. This report describes a technique which was used operationally to produce sea surface temperatures from the NOAA polar orbiting satellites between 1976 and 1981. The single window channel technique used before 1976 is described in the NOAA Technical Memorandum NESS 78 while the multiple window channel technique (MCSST) applied since 1981 is well documented in the scientific literature. This report bridges the gap between these two periods and provides a continuous record of the evolution of one of NOAA's primary satellite derived meteorological products.

I. INTRODUCTION

Sea surface temperature measurements from satellite have been provided routinely by NOAA since the launch of ITOS-1 (Improved TIROS Operational Satellite) in 1970. Before 1975, the operational product was derived from measurements in the 11-12μm spectral window region obtained from a scanning radiometer (SR). The procedure is described in detail in Brower, et al. (1976) and consists of the following steps:

1. Use of a histogram technique to reduce the SR sensor noise (NEΔT = 1.2°C) and to derive a "cloudfree" measurement in a partly cloudy scene at a resolution of 100 km.

2. Correction of the "cloudfree" measurement for atmospheric attenuation with coefficients based on the Vertical Temperature Profile Radiometer (VTPR) sounding product at a resolution of 500 km.

3. Quality control of the observation through a comparison with a smoothed analyzed field of sea surface temperature derived from the satellite data.

The principle problems associated with this procedure are first the gross resolution of the atmospheric attenuation coefficients led to considerable variation in the accuracy of the sea surface temperature measurements and second, the quality control procedure tended to perpetuate errors in the satellite derived analyzed temperature field. Valid observations which could have updated the analyzed field were rejected by the quality control test in regions where the field temperature was in error.

As a result of these problems a new procedure was developed for computing sea surface temperatures and was implemented operationally in April, 1976. This procedure combines single pixel satellite VTPR sounder data at a resolution of 60 km with the SR measurements obtained with the histogram technique. These coincident multi-channel data are used both for cloud detection and for providing corrections for atmospheric absorption in the SR window channel. Those measurements that are determined to be cloudfree are accepted as observations without need for further quality control, eliminating the error persistence problem mentioned previously. This procedure continued to be used operationally until the multi-channel sea surface temperature technique (MCSST) was implemented in November, 1981 with NOAA-7 in the TIROS-N series of satellites. The MCSST procedure uses the multiple window channels of the Advanced Very High Resolution Radiometer (AVHRR) both for cloud detection and for correcting for atmospheric absorption (McClain, et al., 1985). The multiple AVHRR window channels provide a more accurate correction for atmospheric absorption than is possible with the satellite sounder data. Further, the low noise content of the AVHRR (NEΔT

= 0.1°C) eliminates the need for a histogram generation which allows for a much higher density of temperature measurements (8 km resolution).

This report describes the use of relative high resolution single window channel data obtained from a scanning radiometer combined with lower resolution single pixel satellite sounder data for the production of sea surface temperatures. Sections 2 through 4 describe the development of the "combined sensor" procedure from a data base of coincident SR and VTPR data. These sections are lengthy but provide the basis of the general technique.

Section 5 describes the operational implementation of the technique both with the old ITOS satellites and with the new generation TIROS-N and NOAA-6 satellites. Specific operational algorithms are detailed. Operational experience and error sources associated with the "combined sensor", technique are discussed. Section 6 compares the satellite measurements with in situ sea surface temperature measurements such as ship and buoy reports. Emphasis is placed upon a recent satellite-derived sea surface temperature workshop in which the "combined sensor" technique and the currently operational MCSST technique are compared globally with a set of screened ship reports.

2. DATA BASE FOR MODEL DEVELOPMENT

Data for this study have been obtained from the National Oceanic and Atmospheric Administration (NOAA) series of polar-orbiting satellites (viz., NOAA-5), which are environment monitoring satellites operated by the National Environmental Satellite Services (NESS) of NOAA. The NOAA satellite is in a sun-synchronous polar orbit circling the Earth every 115 minutes and providing complete coverage over the globe twice daily. Further details concerning the engineering and orbital characteristics of this satellite system can be found elsewhere (Fortuna and Hambrick, 1974). Data over a 7-day period (July 12-18, 1977) were archived and the regression procedures described herein were applied. Included in this special data base are data from several channels of the Vertical Temperature Profile Radiometer (VTPR) and the atmospheric window channel of the Scanning Radiometer (SR). Since both these instruments scan perpendicular to the orbital track, a dense coverage of data over all ocean areas was obtained.

2.1 VTPR Data

The VTPR is an 8-channel atmospheric sounder. Six of the channels are in the 15μm CO_2 band, and they measure emitted IR radiance from the upper stratosphere (channel 1) to the lower troposphere (channel 6). Also included in the VTPR is a moisture channel in the 18μm H_2O band (channel 7) and an atmospheric window channel at 11μm (channel 8). These data are used primarily to obtain temperature and moisture profiles of the atmosphere (McMillin et al., 1973) but, as will be shown, have important

applications to the computation of sea surface temperatures. The VTPR scan 30.45 degrees to either side of nadir in 23 discrete steps. A ground resolution of 55 km at nadir is achieved with this instrument. The data base consists of a total of 55,175 brightness temperature measurements from the 8-channel VTPR data, along with coincident SR-IR data and a priori sea surface temperature estimates (discussed in 2.3).

2.2 SR Data

The SR onboard the NOAA polar-orbiting satellites provides relatively high resolution (7.4 km at nadir) window-channel data in the 10.5-12.5 μm spectral range. As will be described, these data in conjunction with the sounder data are useful for cloud detection. These data have been collected into approximately 120 x 120 km blocks consisting of 1,024 samples. Frequency histograms are produced for each block over the ocean and an analysis of the higher temperature yields a single retrieval temperature which, hopefully, is representative of that block of the ocean surface (Brower et al., 1976). The retrieval brightness temperature obtained from the SR, along with the nearest spatially and temporally coincident measurement from the sounder, is included in the data archive. Some cloud contamination has been eliminated from the data already by means of quality control procedures based on the shape of the frequency histogram (Brower et al., 1976). However, as will be demonstrated, a considerable amount of cloud contamination remains, and this can be detected using procedures that are described later.

2.3 A Priori Data

Associated with each SR retrieval in the data base is an analyzed field estimate of sea surface temperature; two statistically-independent fields of sea surface temperatures are included. One field is a monthly climatological temperature analysis produced by the National Center for Atmospheric Research (NCAR) on a 2.5° latitude and longitude grid mesh (Washington and Thiel, 1970). The second field is a NESS-produced sea surface temperature analysis derived solely from the NOAA satellite SR-IR data. This analysis is updated daily with new satellite data and is maintained on a 256 x 256 polar-stereographic grid mesh of about 100 km for both Northern and Southern Hemispheres. Details of the procedures for generation and verification of this analysis are described elsewhere (Brower et al., 1976). Recent modifications to these procedures are described separately (Kalinowski et al., 1977). In the subsequent development, the NESS temperature analysis is used for evaluating the accuracy of various algorithms developed for cloud detection as well as estimating atmospheric absorption. The climatological temperatures are used as a parameter in the regression algorithms themselves. Separate temperature estimates are used for these two functions to maintain statistical independence between the parameters included in the regressions and the basis of verification.

3. THE CLOUD PROBLEM

Recognition of the presence of clouds is the single most important function that must be performed in order to obtain accurate sea surface temperature observations from satellite measurements. Use of visible-channel data is an obvious method of cloud detection. Unfortunately, this method can only be used with the daylit half of the data obtained from a polar-orbital satellite. Further, in the daylit portions of the orbit a significant amount of the visible data is contaminated by sun glint. Several techniques exist for detecting cloud contamination solely with IR data that are effective in partly cloudy conditions. These include analyzing a histogram of high resolution data such as is done while producing SR retrievals (Brower et al., 1976; Crosby, 1975). Other techniques include comparing IR window-channel data with different spatial resolution or comparing window-channel data in two different spectral regions (Smith et al., 1974). Unfortunately, none of these techniques can detect uniform cloud cover over the entire retrieval area. The unique characteristic of the cloud detection procedures that are described in this paper is their ability to distinquish a uniform cloud cover from a cloudfree scene with the IR data alone.

3.1 Physical Basis of the Multiple Channel Approach

The ability to detect uniform cloudiness with IR sounder data derives from the fact that the measured brightness temperature difference between two of the tropospheric sounder channels is strongly affected by clouds in the field of view. This effect can be explained partially in terms of the radiative transfer equation, which states that in a uniform scene the measured radiance at the satellite, I, at wavelength ν is composed of a surface term and an atmospheric term, as follows:

$$I_{(\nu)} = B_{(\nu,T_o)}\ \tau + \int_{\tau}^{1} B_{(\nu,T_p)}\ d\tau\ (\nu,P) \qquad (1)$$

With the mean value theorem of the calculus, this equation can be simplified to

$$I_{(\nu)} = B_{(\nu,T_o)}\ \tau + \bar{B}_{(\nu)}\ (1-\tau) \qquad (2)$$

In these equations, T_o and p_o represent the temperature and pressure of the surface, whether it be the sea surface or cloud top; τ is the

transmittance from the surface to the top of the atmosphere; and $\bar{B}$ is a Planck radiance weighted with respect to $d\tau$. This simplified form of the radiative transfer equation is applicable in the 11 μm to 18 μm spectral region of interest because of the following properties of measured radiation in this region:

(1) Clouds may be assumed to be gray, this is, to possess emissivities less than 1.0 and that are independent of wavenumber (McMillin et al., 1973). Consequently, a uniform field of view comprised of a cloud with an emissivity less than unity is mathematically identical to a partly cloudy scene containing black clouds and, as such, only black clouds need to be included in the present discussion.*

(2) The Earth and cloud-reflected sky and solar radiation are negligible compared to the IR emission, and the Earth's ocean surface is very nearly a blackbody (Smith et. al., 1974).

Consider the application of (2) to two different spectral channels, for example the 11.97 μm window and the 14.12 μm upper tropospheric CO_2 channel, of the VTPR. With the window channel, the surface term of the radiative transfer equation dominates in both a cloudfree and cloudy scene because the transmittance to space is nearly unity. With the CO_2 channel, the surface term dominates in a cloudy scene but will be negligible compared with the atmospheric emission term in a cloudfree scene. Therefore, the brightness temperature difference between these channels will be greater in a cloudfree scene than in a cloudy scene. A second effect, which strengthens this relationship, is the usual existence of a temperature inversion at the top of a uniform cloud layer. This phenomenon is so predictable that it is often used to determine cloud-top heights with radiosondes (Byers, 1959). As is shown in Fig. 1, a temperature inversion reduces the brightness temperature difference between the window and CO_2 channels and may, in fact, be crucial for detecting uniform low cloudiness by means of the IR data.

In a partly-cloudy scene the sounder principle described in the preceding paragraphs still applies, but to a lesser degree. It will be shown that a simple application of the sounder principle, coupled with one of the previously mentioned techniques for detecting partly cloudy conditions in the retrieval area, provides an effective means for cloud detection (Parametric classifer). Further, if the sounder principle is applied in a statistically optimal manner, it can stand alone as an effective discriminator (discriminant classifier).

---

* Actually, this is an over simplification because the emissivity of middle-and upper-layer clouds is somewhat less in the 11 μm window than in the 15μm CO_2 spectral region (Gayevsky et al., 1968). However, these assumptions are sufficiently accurate to insure the central premise in this development--that a strong correlation exists between the transmittance through a cloudfree atmosphere and the sensitivity of radiance measured in particular channels to all types of cloud contamination.

3.2 Parametric Classifier

The parametric classifier represents an initial attempt at identifying cloudfree VTPR sounder measurements. It consists of two independent tests, both of which must be satisfied, and involves both the high-resolutuion SR temperature retrieval data and the lower resolution VTPR sounder data:

$$(T_{window} - T_{CO_2})/T_{window} \geq Liml \tag{3}$$

$$ABS(T_{SR} - T_{window}) \leq Lim2. \tag{4}$$

The parameters T_{window}, T_{CO2}, and T_{SR} are, respectively, the brightness temperature measurements in the window, the brightness temperature in one of the tropospheric CO_2 channels of the VTPR, and the derived brightness temperature obtained from the SR-IR data. This first test, (3), is a simple application of the sounder principle. In this form the sounder principle is only effective in identifying contamination by uniform cloud. The second test, (4), compares separate estimates of surface brightness temperature obtained from data in the same atmospheric window region (viz., 10.5-12.5μm) but of differing spatial resolution (i.e., SR vs. VTPR). The difference in data resolution enables this second test (uniformity test) to identify partly cloudy sounder measurements. The sounder principle and the uniformity test, therefore, complement each other to produce an effective cloud discriminator. In the subsequent development of discriminant classifiers, the parametric classifier is used as a first-guess discriminator between cloudfree and cloudy sounder data. Representative values of Liml and Lim2 are given in Sec. 3.3.5.

3.3 Discriminant Classifiers

In this section the development of discriminant functions is described, and it will be shown that they provide a statistically more optimal procedure for applying the sounder principle to cloud detection than that described in Section 3.2. The regression techniques that are developed provide a variety of discriminant functions, some of which use the SR data together with the VTPR sounder data; others that use sounder data together with a priori climatology data; and one that uses window channel data together with the climatology data. The accuracies and special properties of these functions are compared.

3.3.1 Description and Justification of the Regression Method

The general approach is to attempt to find a relationship between two or more channels of the sounder data in a cloudfree scene that is lost in the presence of clouds. It was reasoned that a multiple linear regression against the appropriate parameters (i.e., combinations of VTPR channel measurements, SR data, and a priori data), if restricted to cloudfree scenes, might yield such a useful relationship. A multiple linear regression procedure has been adopted for this purpose, and it attempts to satisfy the following equation for all cloudfree sounder measurements:

$$\sum_i b_i T_{i,n} = C. \tag{5}$$

The regression procedure specifies values of the regression coefficients that minimize, in a least-squares sense, the quantity

$$\sum_n (C - \sum_i b_i T_{i,n})^2. \tag{6}$$

Here C is an arbitrary non-zero constant, b_i is the regression coefficient of the i^{th} term, and $T_{i,n}$ is the value of the i^{th} term obtained from the n^{th} cloudfree measurement of the sounder. This regression is nonstandard in that it does not include a constant coefficient term and the dependent parameter is not a variable. It is important to realize that although the regression will minimize (6) for any choice of parameters, this does not guarantee that the functional relationship is useful for cloud detection. Accordingly, the parameters that are used in the regression analysis are very important.

It is interesting to observe that the function

$$D = \sum_i b_i T_{i,n} \tag{7}$$

is equivalent to, and is subsequently identified as, two-category linear discriminant functions derived from the application of standard statistical discriminant analysis. Standard discriminant analysis, which is described elsewhere (Duda and Hart, 1973), has not been utilized in the present

application because it requires at least two distinct categories in which to place the data. Unfortunately, with the infrared satellite data there is only one well-defined category, namely the cloudfree set of measurements. Even the subset of data consisting of uniform cloud-top measurements does not constitute a well-defined category because of variations in cloud emissivity, cloud height, and cloud type. The primary advantage of a discriminant analysis over the regression analysis is that the former automatically determine, which parameter or combination of parameters within a pre-selected group is most sensitive to cloud contamination within the field of view. However, from the previous discussion of the sounder principle it is clear which parameter may be optimal for this purpose, namely the difference between two specific tropospheric sounder channel measurements.

3.3.2 Selection of Parameters for the Discriminant Functions

For discriminant functions that use sounder data, the primary parameter consists of the difference between two of the VTPR tropospheric brightness temperature measurements. Any combination of the window channel and one of the tropospheric channels in the 15μm CO_2 absorption band can be used, but some work better than others. If the discriminant function is to be an accurate cloud discriminator, this difference term should provide, with some relatively small error, the constant bias C given in (5).

All remaining terms included in the regression analysis provide small positive or negative corrections in order to minimize the variance of the discriminant function when it is applied to cloudfree measurements. A term that is important if the functions are to be applied over large areas of the globe (i.e., polar as well as equatorial regions) is an estimate of sea surface temperature scaled by subtracting a value close to the global mean to not introduce an overall bias to the discriminant function. This estimate may consist of either the high-resolution SR retrieval brightness temperature or the a priori climatlogical temperature. The sounder principle suggests that the brightness temperature difference between certain of the sounder channels is larger in a cloudfree scene than in a cloudy scene. However, due to regional climatic differences in both the temperature and moisture profiles of the atmosphere, the brightness temperature difference between the tropospheric sounder channels in a cloudfree scene is generally smaller in the polar than in the equatorial regions of the globe. This surface term is included to compensate for this effect.

In any locality large temporal variations in the moisture content of the atmosphere can occur. Variations in moisture will influence the brightness temperature difference among the various tropospheric sounder channels. Accordingly, a term incorporating the water vapor channel measurement is included in the regression analysis to compensate for these variations. Similarly, the look angle of the sounder measurement will have an effect on the difference term. Therefore, the secant of the local

zenith angle, scaled by subtracting a value of unity to not introduce a consistent bias in the discriminant function, is included as a fourth term in the analysis. Additional or fewer terms can be included in the regression analysis depending upon the availability of data and the needs of the user.

3.3.3 Regression Analysis

Six different combinations of the VTPR tropospheric channels have been applied in turn as the primary parameter in the various discriminant functions. In all cases the discriminant function is given by

$$D = b_1 \Delta T_{(i-j)} + b_2 (T_{sfc} - 290) + b_3 \Delta T_{(8-7)} + b_4 (\sec(\theta) - 1). \qquad (8)$$

Here, the first term is the primary parameter, consisting of the brightness temperature difference between sounder channels i and j. the parameter T_{sfc} is a sea surface temperature estimate in Kelvin degrees; and θ is the zenith angle of the sounder measurement. The channel numbering convention is that described in section 2.1. The additional measurement, designated 9, represents the independent estimate of sea surface temperature, whether it can be obtained from SR-IR high-resolution data or from the a priori climatological data. The regression procedure minimizes in a least squares sense the quantity

$$\sum_n (1 - D_n)^2, \qquad (9)$$

where the summation is over the cloudfree measurements as determined from the parametric classifier. Of a total of 55,175 separate measurements included in the data base, 23,753 are classified as cloudfree with the parametric classifier. The results obtained with the various discriminant functions are shown in Table 1.

In Table 1, each discriminant function is identified by the combination of channels used in the first term. It is noted that for each combination of channels, two separate discriminant functions are defined: the starred version, which uses the a priori climatological data as an external source of surface temperature in the regression analysis, and the unstarred version, which uses the SR-IR brightness temperature retrieval for this purpose. The last discriminant function, 8-9*, in the table differs from the others in that it uses only the window channel and climatological data in the analysis. This function is included for comparison purposes and to emphasize the flexibility of the regression procedure.

The residuals included in the table are simply an evaluation of (9) for both the cloudfree and cloudy sounder measurements as identified with the parametric classifier. The ratio value is the residual of the cloudy set divided by the residual of the cloudfree set. In general, the discriminant functions with the highest ratios should be the most accurate classifiers.

The β factor is defined as that change in the external estimate of surface temperature that exactly cancels the effect upon the discriminant function of that amount of residual cloud contamination in the sounder data that produces a 1°C error in the window channel. Mathematically, the definition is given by

$$\beta = (\partial T_9/\partial T_8)_D \tag{10}$$

A theorem of Implicit Function in the calculus (Taylor, 1955) allows the expansion of (10) to the form

$$\beta = (\partial T_9/\partial T_8)_D/(\partial D/\partial T_9)_{T_8,T_7\ldots T_1} \tag{11}$$

The denominator in this expression is obtained directly from Table 1. A graphical technique for estimating the numerator is described in section 3.3.4.

In order to detect contamination by uniform cloud with those functions that use the SR retrieval temperature as the external estimate of sea surface temperature, the β parameter must have a value greater than unity since under uniform cloud conditions the error in the retrieval temperature should equal that in the sounder window-channel measurement. Alternatively, because climatology is unaffected by clouds, all of the functions that use climatology as the external source of surface temperature should be able to detect most of the uniform cloud conditions regardless of the of the β parameter. In this case, the β value represents the sensitivity of the discriminant functions to errors in the external data relative to the sensitivity of the former to cloud contamination. It is interesting to compare the value of the β parameter associated with the function 8-9* to that of the functions that include the difference of two tropospheric sounder channels as a parameter. The inclusion of the tropospheric sounder data considerably reduces the effect of errors in the a priori data upon the cloud classification as compared, for example, with a simple threshold test of the window-channel measurement against climatology in which, by definition, the β parameter assumes a value of unity. Obviously, the β parameter represents a fundamental property of the discriminant functions, although its value will vary somewhat depending upon

cloud type and the structure of the temperature profile within the field of view.

3.3.4 Discriminant Analysis

If the discriminant functions are to be useful for cloud detection, then the values of these functions should be highly correlated with the amount of cloud in the field of view of the sounder. It would be very informative and useful to illustrate this correlation graphically. One method of estimating the amount of cloud contamination of the sounder measurements is to correct the window-channel measurement for atmospheric attenuation and then to difference the resultant surface temperature estimate with the NESS-derived SR-IR analysis of sea surface temperature.

The scattergram in Fig. 2, which includes all measurements from the special data base, plots the values of the discriminant function 8-4 as a function of this temperature difference. The statistics below this graph show the mean and standard deviation of the temperature differences for all data having discriminant values within the indicated range. Clearly, the amount of cloud contamination that is rejected in a given application is dictated by the choice of the discriminant function threshold value, a characteristic providing the user with a large degree of flexibility. the linear relationship shown in this graph provides a means for estimating the factor defined in (11). In particular, the total derivative of the discriminant function with respect to errors in the window-channel measurement resulting from cloud contamination can be estimated. However, as is described in Section 4.3, the regression procedures for estimating atmospheric absorption provide temperature corrections that are themselves correlated with the amount of cloud contamination in the sounder data. This correlation has the effect of changing the slope of the linear relatinship indicated in Fig. 2 and biasing estimates of the β factor. Accordingly, the specific regression algorithm for estimating atmospheric absorption has been chosen to minimize this correlation. Further, because the discriminant function 8-9* uses only the window-channel data of the sounder, the β factor can be computed directly from the values of the regression coefficients as well as graphically. These two estimates provide a normalization factor for eliminating the bias that is included in the computation of the β parameter for all other discriminant functions included in Table 1.

The parameter involving the external estimate of sea surface temperature is intended to make the value of the discriminant functions independent of normal climatic atmospheric conditions (i.e., polar versus equatorial conditions). The scattergram in Fig. 3, which shows the values of the discriminant function 8-4 as a function of surface temperature in cloudfree scenes as determined with the parametric classifier, indicates that this goal is achieved. The statistics below this scattergram provide a quantitative measure of the mean values of the discriminant function and

of the variance about the mean. Similar results are achieved with each of the discriminant functions listed in Table 1. The ability to describe a function whose value is strongly correlated with the amount of cloud contamination, but which is independent of sea surface temperature, implies global application. Thus one function provides ability to detect clouds in all regions of the globe and in all seasons of the year.

3.3.5 Error Analysis

With any classification scheme, some of the data are misclassified. In conventional discriminant analysis, a dependent data set is formed in which it is known a priori to which discrete category each data sample belongs. Within the dependent set it is then straightforward to compute the percent misclassification resulting from application of the discriminant functions. In this regression analysis, the dependent data set consists of cloudfree or nearly cloudfree data as determined with the first-guess parametric classifier (see Section 3.2). The attempt is to produce a data set, through the application of the discriminant functions, that contains even less cloud contamination than the dependent data set. It is, therefore, meaningless to compute the percentage of misclassified data based on the dependent data set.

An alternative procedure is to compute the difference between the NESS-derived SR-IR field estimates of sea surface temperature and those calculated from the sounder window-channel measurements corrected for atmospheric absorption, which is a measure of the degree to which the sounder measurements are cloud contaminated. An overall impression of the amount of cloud contamination included in the data set and how much of it is eliminated through the application of the parametric classifier can be obtained from a comparison of Figs. 4 and 5. In these scattergrams the temperature difference is plotted first with all the measurements and secondly with only the cloudfree set. The rather impressive elimination of cloud-contaminated data, indicated by the comparison, is obtained with the parametric classifier as defined in section 3.2. The parameter T_{CO_2} is the VTPR channel-6 brightness temperature measurement at 13.38 μm, and the threshold parameters Lim1 and Lim2 are assigned the values 0.06 and 1.5°C, respectively.

One limitation of the parametric classifier is that the thresholds cannot readily be adjusted to reduce the amount of residual cloud contamination in the set of cloudfree data. If the threshold Lim1 is increased, then no data in the polar regions would be accepted as cloudfree; and if the parameter Lim2 is decreased, then most data in the high-gradient areas over the glove would be rejected. With the discriminant functions, the criteria that determines whether a given sounder measurement is cloudfree or not is simply the magnitude of the parameter D defined by (7). Increasing the threshold value of D makes the discriminant criteria uniformly more restrictive and should reduce the amount of resi-

dual cloud contamination in the cloudfree data set. The optimal choice of the threshold value is dictated by the maximum amount of residual cloud contamination that can be tolerated in a given application.

The most meaningful method to compare the various discriminant functions is to determine the amount of residual contamination as a function of the percentage of measurements in the data base that are classified as cloudfree by the various discriminant functions as the threshold value of D is varied. Such a comparison is shown in Figs. 6 through 9, in which the standard deviation of two independent estimates of the sea surface temperature is the estimator of residual cloud contamination. One of the temperature estimates is the SR-IR field value, and other is the atmospherically-corrected sounder window-channel measurement. Figs. 6 and 7 show the performance of various of the discriminant functions included in Table 1 when they are applied to the complete set of data, whereas Fig. 8 applies to the subset of data that passed the uniformity test defined with (4). All these graphs describe the behavior of the discriminant functions as the threshold value of D is increased.

In approximately the 100-to-60% region, the functions detect the worst cloud contamination, including uniform mid- and upper-level clouds that cannot be detected with the uniformity test. In the 60-to-20% region, the discriminant functions are able to detect the less severe partly-cloudy conditions. With the subset of data relatively little reduction in the standard deviation is achieved in this region, indicating that the uniformity test eliminates most of the data that would otherwise be detected with the discriminant test. In the under 20% region the various discriminant functions exhibit their most characteristic behavior. Surprisingly, the functions 6-5, 5-4, and all other combinations that do not include the window channel, perform worse as the threshold value is increased. Further analysis indicates that this adverse behavior occurs primarily in the polar areas of the globe. The likely explanation is that in this region the functions that include the window channel, such as 8-4 and 8-6, are detecting rather low-level cloudiness, which is not detected with the uniformity test because of the relatively small temperature difference between the cloud top and ocean surface. The functions formed from the 15 m CO_2 channel data are not able to detect very low clouds. In view of the poor results obtained with the function 5-4, it would appear that it has difficulty in detecting even mid-level clouds.

In the foregoing, discriminant functions for the detection of cloud contamination that include as a parameter an estimate of sea surface temperature that is external to the sounder data have been considered. It is relevant to consider the degree of degradation that occurs if the external data source is replaced with the sounder's window-channel measurement. This comparison is shown in Fig. 9. Some degradation does occur because the window-channel measurements include more cloud contamination than either of the two external sources of surface temperature. Nevertheless,

for detecting contamination by uniform clouds, which is very difficult with IR data alone, the sounder-only discriminant functions are quite effective.

4. THE ATMOSPHERIC ATTENUATION PROBLEM

In order to derive sea surface temperatures from cloudfree window-channel data, a correction must be made for the effects of atmospheric absorption. This is easily explained with the radiative transfer equation (1). The first term in this equation is the amount of surface radiance that is transmitted through the atmosphere, whereas the second is the radiance reaching the satellite that is emitted by the atmosphere itself. This latter term is almost always less than the amount of surface radiance absorbed by the atmospheric constituents because temperature generally decreases with increasing height in the troposphere. Consequently, the measured brightness temperatures corresponding to the total radiance reaching the satellite are normally less than the sea surface temperature. Although the 11 μm channel is called an atmospheric window, in a humid atmosphere 50% or more of the satellite-measured radiance is that emitted by the atmosphere itself. Therefore, the method chosen to correct for the absorption effect is critical in the accuracy of the derived sea surface temperatures.

One method of estimating atmospheric attenuation is to perform the integration specified by (1). This procedure will yield a theoretical measurement of satellite-measured brightness temperature in the window channel, which can then be compared with an a priori estimate of sea surface temperature to deduce the temperature correction. Although theoretically correct, this procedure suffers from the need for a considerable amount of a priori knowledge of such factors as temperature and humidity profiles in the atmosphere and the transmittances of the various atmospheric constituents. The satellite sounder data themselves can be applied to compute these meteorological quantities. However, the computation of these quantities from the sounder data is very complex (McMillin et al., 1973), and any inaccuracies will introduce errors in the deduced temperature corrections.

An alternative approach, which is adopted here, is to perform a statistical regression directly against the sounder data to estimate the temperature correction. The major drawback of this technique is that cloud contamination of the sounder data will adversely affect the accuracy of the predicted temperature corrections. The cloud detection procedures for the sounder data, as described in the previous sections, allows one to limit the regression technique to cloudfree sounder measurements and, in these cases, very accurate estimates of the temperature correction can be obtained.

4.1 Physical Basis of Linear Regression Approach

In the 10.5 μm to 12.5 μm spectral region, which includes both the SR-IR window channel and the VTPR window channel, the most important and

variable absorbing constituent in the atmosphere is water vapor. Under most atmospheric conditions, the temperature correction resulting from the presence of carbon dioxide, ozone, and aerosols is considerably less than 1°C (Cogan and Willand, 1976). Consequently, a knowledge of the water vapor content and temperature structure of the atmosphere is all that is needed to obtain an accurate estimate of the temperature correction. In the linear regression approach, data from the VTPR water-vapor channel in the 18-micrometer band is particularly useful, as it is sensitive to both these quantities. Sounder data from the 6.9 μm water vapor absorption band could be used equally well in this application, but the channel should be near the edge of the absorbing band so that radiance upwelling from deep in the troposphere is detected.

A second relationship that is useful for estimating atmospheric attenuation is the generally positive correlation between sea surface temperature and the average or climatological water-vapor content of the atmosphere (Smith et al., 1970), although scatter tends to increase at the higher temperatures. The correlation results primarily from the dependence of the saturation water vapor pressure upon atmospheric temperature (Byers, 1959). This correlation applies to both an a priori climatological estimate of true surface temperature and to the cloudfree satellite window-channel brightness-temperature measurements. However, because the measured brightness temperature is itself affected by the same atmospheric attenuation that is being estimated, the a priori climatological estimate, if available, provides the higher correlation. A comparison of the residuals in Table 2 provides the basis for this statement.

4.2 Regression Development and Parameter Selections

Standard multiple linear regression procedures have been employed to obtain estimates of the temperature correction, $\hat{\Delta T}_n$, with calibrated and cloudfree sounder measurements.

$$\hat{\Delta T}_n = b_o + \sum_i b_i T_{i,n} \tag{12}$$

The symbols b_i and $T_{i,n}$, have the same meanings as in (5). The regression minimizes, in a least squares sense, the quantity

$$\sum_n (\Delta T_n - \hat{\Delta T}_n)^2 , \tag{13}$$

with the summation being only over the cloudfree sounder measurements. The parameter, ΔT_n , is the observed or independently-estimated temperature correction.

Because this regression procedure, as contrasted with that used to derive discriminant functions, includes a constant coefficient term, the scaling of the parameters is not necessary. Further, because the regression equations for estimating the temperature correction are intended to be used only with nearly cloudfree data, the influence of residual cloud contamination is relatively unimportant (see Section 4.3). Consequently, the choice of appropriate parameters is more straightforward in this application than in the development of discriminant functions for cloud detection. The most useful parameter for estimating the temperature correction is the brightness temperature difference between the VTPR water vapor absorption channel and one of the other tropospheric sounder channels. This difference function is very sensitive to variations in water vapor concentrations while minimizing the effects of residual cloud contamination. A second parameter that is important for global applications is an estimate of the sea surface temperature itself. Inclusion of this term enables one regression equation to produce accurate estimates of the temperature correction in all regions of the globe--polar, mid-latitude, and equatorial. A third parameter that obviously should be included is the secant of local zenith angle in order to account for different path lengths through the atmosphere.

4.3 Regression Analysis

Seven different combinations of the VTPR tropospheric channels have been applied as the primary term in the various predictor equations for atmospheric absorption. In all cases, the predictor equator for the temperature correction is given by

$$\hat{\Delta T} = b_o + b_1 \quad \Delta T_{(i-j)} + b_2 \quad \Delta T_{sfc} + b_3 \quad \sec(\theta). \qquad (14)$$

The meanings of the symbols in this equation are the same as in (8) except that here the measurement designated 9 always represents the climatological estimate of surface temperature. The regression procedure minimizes (13), with the summation being over the cloudfree measurements as determined with the discriminant functions (8-4) together with the uniformity test (4). In (13) the parameter ΔT_n is the observed temperature difference between the NESS-produced SR-IR sea surface temperature field analysis and the measured brightness temperature in the VTPR window channel. A rather stringent threshold value of the discriminant function for cloud detection has been chosen; consequently only 11,918 out of a total of 55,175 individual VTPR measurements are included in the regression. The results obtained with the various regression equations for estimating the temperature correction are shown in Table 2.

Each regression algorithm is identified by the combination of channels used in the primary parameter. For each combination of channels, two regression algorithms are defined: The starred algorithm uses the a priori climatology, i.e., measurement 9, as the surface temperature term in the regression analysis, whereas the unstarred algorithm uses the VTPR window-channel 8 brightness temperature measurement. The last two algorithms shown in the table do not include a difference function between VTPR channels in the regression and, therefore, produce only climatological estimates of the temperature correction that are a function of the surface temperature and the look angle of the satellite measurement. Additional parameters have been tested in the regression analysis, such as the absolute brightness temperature measurements in several of the tropospheric sounder channels, and a term that is a quadratic function of the sea surface temperature estimate. Although these additional parameters always reduce he residuals shown in Table 2, as is explained in Section 4.4, it does not follow that the predicted temperature corrections are therefore improved.

The residuals shown in Table 2 are an evaluation of (13) for both the clear and cloudy measurements identified with the discriminant function 8-4 described previously. In comparing the residuals of various algorithms, it must be emphasized that these calculated values, as well as derived statistical quantities, are sensitive not only to the accuracy of the algorithm's estimate of the temperature correction but also to any correlation between the estimated temperature correction and residual cloud contamination in the sounder data. As a result of this correlation, the algorithm 6-5*, which does not use the water vapor channel data, has one of the lowest cloudfree residuals in Table 2 because it is correcting for residual cloud contamination (see Section 4.4). A measure of this correlation is provided by the γ factor, whose value represents the decrease in the predicted temperature correction resulting from that amount residual cloud contamination of the sounder data required to produce a 1°C error in the window channel. Mathematically, this factor is defined by,

$$\gamma = + \, d \, \hat{\Delta T}/dT_8. \tag{15}$$

Obviously, in order to properly compare the various regression algorithms for estimating the temperature correction, differences in this correlation factor must be considered. Such a correlation analysis is provided in the following section. It is observed from Table 2 that the algorithm 7-6* has one of the smallest correlation factor values and, for this reason, it was utilized in the verification of the various discriminant functions for cloud detection (Section 3.3.4). A second distinquishing characteristics of the various regression algorithms in Table 2 is their relative dependence upon the surface temperature estimate. It is apparent that Table 2 includes algorithms for estimating the temperature correction that vary con-

siderably in their characteristics. The user must determine which algorithm is best suited to his needs.

4.4 Correlation Analysis

The difference in temperature between the SR-IR sea surface field analysis temperature and the sounder window-channel measurement, corrected for atmospheric absorption with one of the regression algorithms included in Table 2, arises from three types of error. These are errors in the SR-IR field estimate of sea surface temperature, errors in the sounder measurement resulting primarily from cloud contamination, and errors in the predicted values of the temperature correction. Mathematically, the total error can be expressed by

$$\tilde{\varepsilon}_{tot} = \tilde{\varepsilon}_{SR} - \tilde{\varepsilon}_{m} - \tilde{\varepsilon}_{\Delta T} , \tag{16}$$

with the wavy lines over these terms indicating that statistically they are random variables. Correspondingly, the error in the predicted value of the temperature correction for atmospheric absorption can be expressed by

$$\tilde{\varepsilon}_{\Delta T} = \tilde{\varepsilon}_{o} + \gamma\tilde{\varepsilon}_{m} , \tag{17}$$

where $\tilde{\varepsilon}_{o}$ represents the lack of fit of the regression algorithm in a cloudfree scene resulting, perhaps, from variations in the vertical profiles of temperature and moisture; $\tilde{\varepsilon}_{m}$ is the brightness temperature error in the sounder window channel measurement resulting from cloud contamination; and γ is the correlation coefficient defined by (15). Substituting from (17) into (16), one obtains

$$\tilde{\varepsilon}_{tot} = \tilde{\varepsilon}_{SR} - (1 + \gamma)\,\tilde{\varepsilon}_{m} - \tilde{\varepsilon}_{o} . \tag{18}$$

Statistical theory states that the variance of a linear combination of random variables is obtained from the sum of squares of the individual terms plus the covariance between terms (Freund, 1971). Since the random variables $\tilde{\varepsilon}_{SR}$, $\tilde{\varepsilon}_{m}$, and $\tilde{\varepsilon}_{o}$ are statistically independent, the variance is given simply by

$$\sigma^2_{tot} = \sigma^2_{SR} + \sigma^2_{m}\,(1 + \gamma)^2 + \sigma^2_{o} . \tag{19}$$

Similarly, the variance of the error in the predicted temperature correction is given by

$$\sigma^2_{\Delta T} = \sigma^2_o + \gamma^2\sigma^2_m \ . \tag{20}$$

Substituting from (20) into (19), one obtains

$$\sigma^2_{\Delta T} = \sigma^2_{tot} - \sigma^2_{SR} - \sigma^2_m (1 + 2\gamma) \ . \tag{21}$$

The residuals provided in Table 2 are measured values of the parameter σ^2_{tot}.

The relationship described by (21) allows one to compare the relative accuracies achieved in estimating the temperature correction with the various regression algorithms. Absolute accuracies cannot be determined because the parameters σ^2_{SR} and σ^2_m are not known. The variance of the error in the predicted estimates of temperature correction, $\sigma^2_{\Delta T}$, obtained with the various regression algorithms is plotted in Fig. 10 as a function of the variance of the error in the brightness temperature measurements, σ^2_m . The values of the correlation coefficients, γ , used in this graph are listed in Table 2. To interpret this figure, assume that the actual variance of measurement in this data is $1.5°C^2$. Then the algorithm 8-7* provides the lowest variance of the error of prediction. If an additional cloud filter were applied to the data that removed all cloud contamination, this algorithm would provide the lowest total observed variance, σ^2_{tot}. If instead the variance of measurement of the actual data is only $0.5°C^2$, then the algorithm 9-7* provides the lowest total observed variance regardless of whether the cloud contamination is removed or not. Whereas either algorithm 9-7* or 8-7* are best overall in minimizing the variance of the error in the predicted temperature correction, the optimal choice of a regression algorithm depends upon its application. An algorithm with a very small γ value minimizes the effect of residual cloud contamination upon the predicted temperature correction, whereas one

with a negative γ factor weakens the effect of residual cloud contamination upon the estimation of sea surface temperature.

Since one cannot calculate the γ factor directly from (15), the correlation coefficients, γ, have been estimated for each of the regression algorithms included in Table 2 with the aid of (19), which is applicable to each of the algorithms and to any subset of data. Considering the set of cloud data for which the observed residual σ^2_{tot} is given in Table 2, it is apparent that the cloud-induced variance, σ^2_m, is the primary contributor to the total observed residual. Accordingly, one may approximate γ by

$$\gamma = (\sigma^2_{tot}/\sigma^2_m)^{1/2} - 1 \ . \qquad (22)$$

If the correlation coefficient, γ, is known a priori for any of the regression algorithms, this equation can be applied to first obtain an estimate of σ^2_m and subsequently provide estimates of γ for all the other regression algorithms. The regression algorithm (9) provides the needed a priori information since it does not use any of the sounder data and, therefore by the definition given in (15), the correlation coefficient must be zero. The algorithm (8) provides a measure of the accuracy of (22) since in this case, by definition, the correlation coefficient equals the regression coefficient of the surface term.

4.5 SR-IR Sea Surface Temperature Analysis

In the regression procedure for estimating the temperature correction, the temperature difference between the SR-IR sea surface temperature field analysis value and the window-channel measurement of the sounder is used as the dependent variable. In the scattergram shown in Fig. 11, this difference parameter in the cloudfree scenes is plotted as a function of the surface temperature. Correspondingly, the predicted temperature correction obtained with regression equation 8-7* is plotted as a function of surface temperature in Fig. 12. The statistics that follow these scattergrams provide a comparison of the observed and predicted mean temperature corrections as a function of sea surface temperatures over the globe. These mean corrections agree closely and, as is expected from physical principles, increase with increasing surface temperature. The difference in the variability of the temperature corrections at any given surface temperature is significant, being much larger in the observed data sets. This is not unexpected since the observed data includes not only the effect of variations in moisture and temperature profiles, but also errors in the SR-IR sea surface temperature analysis and in the window-channel measurements.

It is useful to compare the variability of these predicted temperature corrections with a theoretical treatment of varying moisture and tem-

perature conditions. Such a treatment exists for the 8 to 12μmicrometer spectral window region that includes the VTPR window channel (Wark et al., 1962). Outgoing radiance was computed for 102 model atmospheres (i.e., temperature and humidity profiles from radiosonde data obtained over all seasons and latitudes). A consideration of the effect of water vapor alone indicates that the temperature correction should have a variation of approximately 2°C in polar regions, increasing the perhaps 6°C in tropical latitudes. This result is in reasonable agreement with the variation of the predicted temperature corrections shown in Fig. 12. However the theoretical value may be underestimated in moist atmospheres since water vapor continuum absorption has not been properly accounted for. On the other hand, both the theoretical treatment and observed SR-IR data indicate that in the presence of an atmospheric temperature inversion a negative temperature correction, rather than a positive one, may be needed. This relatively rare occurrence is not accounted for in the regression treatment. A more recent theoretical treatment of the problem, specifically dealing with the SR window channel of the NOAA series of satellites, indicates that the expected temperature correction resulting from the presence of both carbon dioxide and water vapor increases from 2.5°C in a dry polar atmosphere to 10.5°C in a moist tropical atmosphere (Maul and Sidran, 1973). These values are in good agreement with the data shown in Figs. 11 and 12.

In summary, the regression approach for estimating the temperature correction in cloudfree scenes appears highly successful under normally occurring atmospheric conditions over the globe. The advantage of this method over the more theoretical approach of integrating the radiative transfer equation is that relatively little a priori atmospheric information is needed to derive an accurate estimate of the correction.

5. OPERATIONAL IMPLEMENTATION

The procedures described in sections 2-4 have been applied operationally both with the ITOS series of satellites (NOAA-4 and NOAA-5) and with the TIROS-N series of satellites (TIROS-N and NOAA-6). With NOAA-4 and NOAA-5 the parametric classifier alone was used for cloud testing (section 3.2). NOAA-4 failed in September 1976 soon after the implementation of the "combined sensor" technique whereas NOAA-5 remained operational for one and a half years until the SR instrument failed in March 1978. During this time frame a consistent atmospheric correction algorithm was applied to the "cloudfree" data; namely, 9-7* given in Table 2. When the cloud tests indicated that the sounder data was "cloudy", an attempt was made to measure the sea surface temperature with the SR alone in order to fill in data voids. However, because of the likelihood that the SR measurement was cloud contaminated and because there was no reliable way to correct the measurement for atmospheric attenuation, these measurements were assigned a low reliability. The method employed of combining "different types" of observations is described in Walton, et al., 1976. Between March 1978 and February 1979,

when TIROS-N became operational, experimental sea surface temperature observations were computed with the VTPR data alone.

With the TIROS-N series of satellites, the Advanced Very High Resolution Radiometer (AVHRR) replaced the SR and the High Resolution Infra-Red Sounder (HIRS) replaced the VTPR. A complete description of these instruments is given in Schwalb, 1978. Although the "combined sensor" technique remained consistent when TIROS-N became operational, a considerable improvement in accuracy of the satellite derived sea surface temperatures was realized. This improvement arises from three sources:

1. The TIROS-N AVHRR and HIRS data are of much higher quality than the corresponding data from the ITOS satellites (NEΔT of 0.1°C for 11μm AVHRR channel vs. 1.2°C for SR and 18 km resolution for HIRS data vs. 50 km for VTPR).

2. The discriminant function algorithm is used for cloud detection. The linear algorithm is as described in Section 4 but with appropriate HIRS channels replacing the VTPR channels.

3. A statistical Maximum Likelihood Technique (MLT) is applied to 11 x 11 arrays of 4-km resolution AVHRR 11μm data to provide a single "cloudfree" measurement at a 50 km interval. (Crosby, D.S. 1975).

The "combined sensor" technique was applied to TIROS-N in March 1979, to NOAA-6 in January 1980 and finally was replaced with the MCSST technique shortly after NOAA-7 became operational in November 1981. Success with the MCSST technique came only with NOAA-7, which had a 5 channel AVHRR instrument, because the earlier four channel instruments had severe noise problems associated with the 3.7μm window channel making that channel nearly useless for quantitative processing.
Unfortunately, the HIRS 3.7μm window channel measurement, which could have provided a dual window atmospheric correction algorithm, was not utilized in the "combined sensor" technique. Unlike the MCSST technique, there was no provision for separate daytime and nighttime algorithms and the 3.7μm near IR window channel is subject to contamination by reflected solar radiation in the daytime.

5.1 Generation of Regression Algorithms for TIROS N and NOAA 6

After the launch of TIROS N and NOAA 6, two days of global data were collected in order to perform the multiple linear regression defined by eqn. 3. A set of threshold tests were applied to eliminate most of the cloud contaminated data:

1. The AVHRR 11μm "cloudfree" measurement must not differ by more than 2°C from the HIRS window channel measurement (H8), the 11μm channel.

2. The HIRS channel difference, H8-H7, must exceed 17°, where H7 is a lower tropospheric sounding CO_2 channel measurement at 13.35μm.

These tests form the so-called parametric classifier described in Section 3.2. The designation H8, H7, etc. conform to the HIRS channel numbering convention (Schwalb, 1978). The data that passed these tests were applied in the regression procedure, resulting in the following discriminant functions for TIROS N and NOAA-6:

$$\begin{aligned} D = &- 0.00996\ (\text{climatology} - 290°K) \\ &+ 0.0225\ (H8-H5) \\ &+ 0.00217\ (H10-H11) \\ &-0.185\ (\sec(\theta)-1) \end{aligned} \qquad \text{TIROS-N} \qquad (23)$$

$$\begin{aligned} D = &- 0.00688\ (\text{climatology} - 290°K) \\ &+ 0.0235\ (H8-H5) \\ &+ 0.00160\ (H10-H11) \\ &- 0.177\ (\sec(\theta) -1) \end{aligned} \qquad \text{NOAA-6} \qquad (24)$$

Climatology in these equations is the NCAR monthly mean climatology temperature coincident with the satellite measurement (Washington, and Thiel, 1970); H5 is a HIRS CO_2 middle tropospheric sounding measurement at 13.97μm while H10 and H11 are water vapor sounding measurements centered at 8.16μm and 7.33μm, respectively; secant (θ) is the zenith angle of the satellite measurement. For independent satellite data to be classified as cloudfree, the value of D must be between 0.98 and 1.20 and the two threshold tests described above must be satisfied. These functions are identical in form to those generated with the VTPR data which are given in Table 1. The term involving (H8-H5) is equivalent to (8-4) or (8-5) of the VTPR. The term involving (H10-H11) has no spectral equivalence with the VTPR but produces a water vapor correction as does the term Δ T(8-7) of the VTPR. Generally the coefficients of these HIRS discriminant functions are between those generated with the functions 8-4* and 8-5* of the VTPR.

A useful measure of the cloud detection ability of these HIRS discriminant functions is to apply the discriminant test to daytime data only and to measure the mean bi-directional reflectance of visible channel data coincident with the infrared data passing the test as the minimum threshold

of the discriminant function is varied. Data for this analysis has been obtained from NOAA-6, the second satellite in the TIROS-N series (Schwalb, 1978). The data consisted of a morning pass through the mid-Pacific in mid-October, 1980. The results of the reflectance measurements are shown in Fig. 13. Standard NESS calibration procedures have been used for converting the visible channel output to a reflectance measurement (Lauritson et al., 1979). The only cloud screening of this data is provided by the discriminant function used operationally which is described in the previous paragraph. The reflectance measurements are obtained from individual samples of AVHRR visible band data having a resolution of 4 km and located at the center of each HIRS sounder measurement, the latter having a resolution of 17 km at nadir. The effect of sun glint has been minimized by not including data with a satellite zenith angle greater than 20° when scanning to the East (toward the sun). The curve to the left indicates the mean reflectance values of the data passing the test, i.e., percent cloudfree as the threshold of the discriminant function is increased toward unity. The average reflectance of all the data is 25% although the reflectance drops rapidly as the percentage of data passing the test decreases. Furthermore the limiting reflectance value of 5 or 6 percent is indicative of a cloudfree sea surface. The curve to the right shows the reflectance values of the remaining data failing the test as the threshold is reduced. This curve indicates that when only 10% of the data fail the discriminant test, the mean reflectance of that 10% is 55 percent, which is indicative of a cloud-filled field of view. The similarity of this figure to figures 6-9, which apply to several of the VTPR discriminant functions but which use a statistical measure of cloudiness, is notable.

After the HIRS discriminant function is computed, the two days worth of data are screened with the discriminant test. All the data passing are then applied in a multiple linear regression to compute temperature corrections, Δt, for atmospheric absorption. The following algorithm correct the AVHRR 11μm window channel "cloudfree" measurement for atmospheric absorption, providing an estimate of sea surface temperature:

$$\Delta T = -14.99 + 0.0470\,(100\text{ km field SST}) + 0.1257\,(100\text{ km field SST} - \text{H11}) + 1.047\,(\text{secant}\,(\theta) - 1) \qquad \text{TIROS-N} \qquad (25)$$

$$\Delta T = -19.64 + 0.0604\,(100\text{ km field SST}) + 0.1532\,(100\text{ km field SST} - \text{H11}) \qquad (26)$$

+2.138 (secant (θ) -1) NOAA-6

In these equations the 100 km field SST is an analyzed field of sea surface temperature derived solely from the AVHRR/HIRS satellite data (Kalinowski et al. 1977); H11 is a HIRS mid-tropospheric water vapor measurement centered at 7.33 m; and secant 0 is the zenith. This algorithm is identical in form to those generated with the VTPR data as described in Table 2 although the HIRS water vapor channel, H11, is in a different spectral region than is the VTPR water vapor channel, channel 7 (the central wavelengths are 8.7μm for the VTPR channel and 7.3μm for the HIRS channel). A comparison of the ability of various combinations of HIRS Channels to predict atmospheric water vapor is shown in Fig. 14.
This figure, obtained from transmittance simulations, indicates that the combination SST-H_{11} is the most sensitive to water vapor especially at high concentrations. Because the coefficient of this term in eqn. 25 is much less than unity a-priori errors in the 100 km field SST damp out very rapidly with the injection of new satellite data into the analysis.

5.2 Operational Experience

Operational experience with the "combined sensor" technique has pointed out certain problems, some of which are relatively minor while others have required modifications to the basic processing technique described in the previous sections. A systems events and messages log which lists all changes to the operational processing between October, 1978 and February, 1982 is given in Appendix A.

Three significant error sources associated with the "combined sensor" technique have been identified. First, a negative bias of the satellite estimates relative to AXBT's (airborne expendable bathythermographs) was found in the tropical Pacific (Barnett et al., 1979). This error is apparently inherent to the "combined sensor" technique and is related to broken cloud conditions within the field of view of the sounder data. After implementation of the discriminant procedure in 1979 a correction was applied that consists of simply increasing the minimum threshold of the discriminant function in tropical regions. This correction has had the dual effect of considerably reducing both the negative bias, as determined from comparisons with ship reports, which is good, and the coverage of satellite-based SSTs in these regions, which is not desirable. Figure 15 which is discussed in detail in Section 6 clearly shows significant data voids in the tropical latitude zone during November 1979.

A second problem that has been identified is a warm bias of one or more degrees centigrade in the satellite measurements of SST in the middle and polar latitudes of the summer hemisphere. Two separate sources can contribute to this problem. First, solar ocean surface warming under low wind conditions during the daytime produce an apparent bias between ship

bucket measurements and satellite skin measurements. This surface effect has also been observed with the MCSST data (McClain E.P., et al. 1985). A second cause is associated with a relatively low temperature lapse rate in the lower troposphere in the higher latitudes of the summer hemisphere. Under these conditions the temperature correction algorithms, which utilize a middle tropospheric water vapor channel, H11, provide too large a correction for atmospheric absorption resulting in the error (Simulations show that the MCSST algorithms utilizing two or three window channels automatically adjust for lapse rate changes). A correction for this bias in the "combined sensor" technique, based upon atmospheric temperature lapse rate information obtained from the HIRS data was implemented in August 1980. This correction appears to have dramatically reduced the warm bias in the high latitudes without adversely affecting other regions (Walton, 1982).

A third problem with the "combined sensor" technique which is closely related to the second is a lack of coverage of satellite measurements in the polar regions of the summer hemisphere which, for the November, 1979 period represented in Fig. 15, is the southern hemisphere. Near isothermal or even inversion atmospheric lapse rate conditions, which are common in the summer hemisphere, will cause the discriminant test to be failed whether or not clouds are present as is demonstrated in Fig. 1. No attempt to correct this problem was attempted since any relaxation of the discriminant threshold value would lead to increased cloud contamination in regions where the lapse rate was nominal. A further discussion of the errors associated with the "combined sensor" technique is given in Appendix B.

6. COMPARISON WITH IN SITU DATA

A recently completed set of three sea surface temperature workshops (NASA/JPL, 1983, 1984, 1985) provides some measure of the accuracy of both the "combined sensor" technique as well as its replacement, the MCSST technique. The intent of the workshop was to inter-compare the accuracy associated with different satellite instruments and algorithms used to measure sea surface temperatures, the NOAA Polar Orbiting Satellite product being one of those chosen for this study. The comparison covered four separate monthly periods: November 1979, December 1981, March 1982 and July 1982. Comparison with in situ data provide accuracy estimates of the "combined sensor technique" during the first period and of the MCSST technique in the latter periods.

6.1. In Situ Data and Data Analysis

Ship measurements of sea surface temperature were obtained from the Fleet Numerical Oceanography Center (FNOC). These measurements provide good coverage in the Northern Hemisphere and fair coverage in the Southern Hemisphere, although the quality of the measurements is variable. As a result, a screening procedure was developed involving the use of climato-

logy which greatly improved the quality of this data but which limited its use to the Northern Hemisphere almost exclusively (NASA/JPL, 1984).

A set of XBT reports were also obtained from FNOC for each of the study periods. The quality of this data set is presumably very good but is limited to the North Pacific, and even there the coverage is spotty.

A third set of in situ data available only for the November 1979 study period is temperature reports from over a hundred FGGE drifting buoys in the Southern Hemisphere. The coverage is excellent in the Southern Hemisphere. Unfortunately this data is not screened and independent studies have indicated that some of these reports are faulty.

Each of these data sources as well as the satellite temperature measurements are organized in two degree latitude/longitude bins. "Raw" anomaly values are obtained by subtracting the Reynolds temperature climatology, interpolated to the position of the satellite or in situ measurement (Reynolds, 1982). The final product for each data source is a two degree mean monthly anomaly field.

Figure 15 shows the resulting temperature anomalies of the TIROS-N operational product in November 1979. Additionally, is shown the anomalies of the ships, XBTs and FGGE buoys. This figure also illustrates the data coverage obtained with each of these sources (black representing a data void). This figure is a gray shade rendition of a color photograph provided in the third workshop report. In this rendition the dark gray (as opposed to black) indicates negative anomalies while the light gray represents positive temperature anomalies.

6.2 Statistical Analysis

The third Sea Surface Temperature Workshop report contains a number of statistical tables which specify the bias and scatter of the satellite measurements relative to the a priori and in-situ measurements. These statistics are computed from the monthly mean anomaly fields, each bin providing one data point for the analysis. A given bin is included in the analysis only if both the satellite and in-situ data had a measurement at that location. Table 3 summarizes the global and regional analyses for the Nov. 1979 and Dec. 1981 study periods. This table not only provides accuracy estimates of the satellite measurements against in-situ data, it also provides a useful comparison of the MCSST and "combined sensor" techniques for estimating sea surface temperature.

A few comments concerning this table concludes this report. The comparison against climatology indicates that the "combined sensor" temperatures are approximately half a degree centigrade warmer than those obtained with the MCSST algorithms. The number of bins used in the analysis against climatology is reflective of the data coverage achieved with

the satellite while in the other comparisons it is reflective of the data coverage of the in situ data. In both study periods the scatter of the satellite measurements is smallest in the comparison with the Pazan ship reports. These ship reports are the only in situ data to be screened with a comparison with climatology to remove faulty reports. Further, a minimum of five ship measurements within a two degree latitude/longitude bin were required for that bin's anomaly value to be included in the statistical analysis. Consequently the Pazan ships probably provide the most accurate ground truth estimates in this study.

The table shows that the "combined sensor" technique provides a scatter against the Pazan ships nearly as low as the MCSST technique. This somewhat surprising result may be partly due to the way the data is analyzed. Since all the data is placed in two degree bins, the higher resolution of the MCSST data (8 km vs. 20 km) is of no benefit in the data analysis. Further the timing of this study (late fall in the Northern Hemisphere) is advantageous to the "combined sensor" technique. As described in Section 5.2, most of the problems associated with the "combined sensor" technique occur in the higher latitudes of the summer hemisphere. Although corrective modifications to the operational processing of NOAA-6 data were made, some degradation of these statistics might occur in a summer study period, especially with TIROS-N data. The relative large scatter against climatology in the South Pacific and against the FGGE buoys may be indicative of this effect in the Southern Hemisphere, although part of the scatter is probably due to the fact that the FGGE buoy data are unscreened.

In summary, the JPL sea surface temperature workshops have provided the first independent and global study of the accuracy achieved with the "combined sensor" and MCSST techniques for measuring sea surface temperature from space. It provides a reliable comparison between these techniques on a monthly mean basis because consistent data processing procedures were applied in all study periods. There has been a continuing need for a through description of the "combined sensor" technique and of the accuracy which it achieves. It is hoped that this report and the JPL workshop reports fill this need.

ACKNOWLEDGEMENT

W. Pichel of NOAA/NESDIS compiled the material given in Appendix A of this report. W. Pichel and B. Brower also of NOAA/NESDIS compiled most of the material given in Appendix B. Madelyn Bowman prepared this manuscript for printing. E. Paul McClain and Dave McGinnis reviewed the text.

References

Barnett, T.B., Potzert, W.C., Webb, S.C., and Bean, B.R., 1979: Climatological Usefulness of Satellite Determined Sea Surface Temperatures in the Tropical Pacific. Bull. Am. Meteorol. Soc., 60, 197-205.

Brower, Robert L., Gohrband, Hilda S., Pichel, William G., Signore, T.L., Walton, C.C., 1976: Satellite derived sea surface temperature from NOAA spacecraft. NOAA Tech. Memo. NESS 78, 74 pp.

Byers, H.R., 1959: General Meteorology, New York, N.Y., McGraw Hill Book Company, 107.

Cogan, J.L. and J.H. Willand, 1976: Measurement of sea surface temperature by the NOAA-2 satellite. J. Appl. Meteor., 15, 173-180.

Crosby, D.S., 1975: Obtaining estimatd clear radiances when some of the fields of view are cloud contaminated. Proceedings of the Fourth Conference on Probability ans Statistics in Atmospheric Sciences, Tallahassee, Fla., 163-164.

Duda, R.O. and P.E. Hart, 1973: Pattern Classification ans Scene Analysis. New York, N.Y., John Wiley & Sons Inc., 20.

Fortuna, J.F. and L.N. Hambrick, 1974: The operation of the NOAA polar satellite system. NOAA Tech. Memo. NESS 60, 127 pp.

Freund, J.E., 1971: Mathematical Statistics. Englewood Cliffs, N.J., Prentice Hall, Inc., 195.

Gayevsky, V.L., L.N. Guseva, K. Ya. Kondratyev, Ye. P. Novoseltsev, N. Ye. Ter-Markaryantaz, and V.F. Zhvalev, 1968: Meteorological Interpretation of infrared pictures of the Earth from space. Pure and Appl. Geophys., 69, 336-359.

Kalinowski, J. Keith, T.L. Signore W.G. Pichel, C.C. Walton, R.L. Brower, S.R. Brown, and K.G. Bennekamper, 1977: Present and future operational NOAA satellite oceanographic products: an introduction. Proceedings of Eleventh International Symposium on Remote Sensing of Environment, Ann Arbor, Mich., 625-633.

Lauritson, L., Nelson, G.J., and Porto, F.W., Data Extraction and Calibration of TIROS-N/NOAA Radiometers, NOAA Technical Memorandum NESS 107, U.S. Dept. of Commerce, Washington, D.C. 73 pp., 1979.

Maul, G.A. and Sidran, 1973: Effects on ocean surface temperature sensing from the NOAA satellite scanning radiometer. J. Geophys. Res., 78 (12), 1909-1916.

McClain, E.P., W.G. Pichel, and C.C. Walton, 1985: Comparative Performance of AVHRR-Based Multichannel Sea Surface Temperatures. Jour. of Geophy. Res., 90, 11587-11601

McMillin, L.M., D.Q. Wark, J.M. Siomkajld, P.G. Abel, A. Werbowetzki, L.A. Lauritson, J.A. Pritchard, D.S. Crosby, H.M. Woolf, R.C. Luebbe, M.P. Weinreb, H.E. Fleming, F.E. Bittner, and C.M. Hayden, 1973: Satellite infrared soundings from NOAA spacecraft. NOAA Tech. Rept. NESS 65, 112 pp.

NASA/JPL, Satellite-Derived Sea Surface Temperature: Workshop I, January 27-28, 1983, Pasadena, Caif.; JPL Public. 83-34, Jet Propulsin Lab., Pasadena, CA., 1983.

NASA/JPL, Satellite-Derived Sea Surface Temperature: Workshop II, June 22-24, 1983, Pasadena, Califrnia: JPL Public. 85-5, Jet Propulsion Lab., Pasadena, CA, 1984.

NASA/JPL, Satellite-Derived Sea Surface Temperature: Workshop III, Feb. 22-24, 1984, Pasadena, California: JPL Public. 85-63, Jet Propulsion Lab., Pasadena, CA., 1985.

Reynolds, R., A Monthly Averaged Climatology of Sea Surface Temperature, NOAA Tech. Rep. NWS 31, U.S. Dept. of Comm., Silver Spring, MD, 1982.

Schwalb, Arthur, 1978: The TIROS-N/NOAA A-G satelite series. NOAA Tech. Memo. NESS 95, 75 pp.

Smith, W.L., P.K. Rao, R. Koffler, and W.R. Curtis, 1970: The determination of sea surface temperature from satellite high resolution infrared window radiation measurements. Mon. Wea. Rev., 98 (8), 604-611.

Smith, W.L., H.M. Woolf, P.G. Abel, C.M. Hayden, M. Chalfant, and N. Grody, 1974: NIMBUS-5 sounder data processing system. NOAA Tech. Memo. NESS 57, 99 pp.

Taylor, A.E., 1955: Advanced Calculus. New York, N.Y., Ginn and Company, 187-191.

Wark, D.Q., G. Yamamoto, and J.H. Lienesch, 1962: Methods of estimating infrared flux and surface temperature from meteorological satellites. J. Atmos. Sci., 19 (5), 369-384.

Walton, C.C., Brower, R.L., and Signore, T.L., Satellite-Derived Sea Surface Temperatures by Multi-Channel Regression, Proceed. of

COSPAR Symposium on Meteorologicall Observations from Space, COSPAR XIX, Philadelphia, Pa., 155-159, June 8-10, 1976.

Walton, C., Recent Improvements in Deriving Sea Surface Temperatures from th NOAA-6 Satellite System, IEEE Transactions on Geoscience and Remote Science, GE-20 #3, 404-408, July 1982.

Washington, W.M. and L.G. Thiel, 1970: Digitized global monthly mean ocean surface temperatures. NCAR Tech. Notes NCAR-TN-54, 30 pp.

TABLE 1

Regression term	ΔT(i-j)	Regression Coefficients T_{sfc}-290	ΔT(8-7)	Sec θ-1	Residuals Clear	Cloudy	Ratio	Parameter β
8-6	$+0.53154\times10^{-1}$	-0.94000×10^{-2}	-0.63170×10^{-2}	-0.44658	0.00276	0.02921	10.6	2.4
8-6*	$+0.53927\times10^{-1}$	-0.79555×10^{-2}	-0.48435×10^{-2}	-0.39008	0.00367	0.04357	11.9	2.8
8-5	$+0.28431\times10^{-1}$	-0.84752×10^{-2}	$+0.14546\times10^{-3}$	-0.32472	0.00159	0.02446	15.4	2.2
8-5*	$+0.28823\times10^{-1}$	-0.72413×10^{-2}	$+0.15724\times10^{-2}$	-0.27614	0.00225	0.03552	15.8	2.6
8-4	$+0.18917\times10^{-1}$	-0.91160×10^{-2}	$+0.78542\times10^{-3}$	-0.22532	0.00095	0.01928	20.3	1.9
8-4*	$+0.19149\times10^{-1}$	-0.80851×10^{-2}	$+0.25656\times10^{-2}$	-0.17310	0.00159	0.02927	18.4	2.1
6-5	$+0.59482\times10^{-1}$	-0.78144×10^{-2}	$+0.88816\times10^{-2}$	-0.15763	0.00137	0.02168	15.8	2.5
6-5*	$+0.60202\times10^{-1}$	-0.69447×10^{-2}	$+0.10425\times10^{-1}$	-0.11507	0.00181	0.02999	16.6	2.8
6-4	$+0.28692\times10^{-1}$	-0.92682×10^{-2}	$+0.58921\times10^{-2}$	-0.81866×10^{-1}	0.00093	0.01661	17.9	1.8
6-4*	$+0.29012\times10^{-1}$	-0.84631×10^{-2}	$+0.79268\times10^{-2}$	-0.30717×10^{-1}	0.00144	0.02480	17.2	2.0
5-4	$+0.54520\times10^{-1}$	-0.10816×10^{-1}	$+0.39746\times10^{-2}$	$+0.23280\times10^{-2}$	0.00120	0.01379	11.5	1.5
5-4*	$+0.55092\times10^{-1}$	-0.10065×10^{-1}	$+0.65273\times10^{-2}$	$+0.62332\times10^{-1}$	0.00179	0.02174	12.1	1.6
8-9*+40°C	$+0.28080\times10^{-1}$	$+0.51529\times10^{-2}$	-------	+0.21991	0.00397	0.07041	17.7	1.2

Table 1. A statistical description of various discriminant functions produced for cloud detection.

TABLE 2

Regression parameter	Regression Coefficients ΔT	T_{sfc}	Sec θ	Constant	Residuals Clear	Cloudy	Ratio	Correlation γ
9-7	+0.32265	$+0.13980\times10^{-1}$	$+0.29590\times10^{+1}$	$-0.88295\times10^{+1}$	1.71	38.52	22.5	-0.23
9-7*	+0.29857	$+0.35610\times10^{-1}$	$+0.28495\times10^{+1}$	$-0.14634\times10^{+2}$	1.68	39.14	23.3	-0.22
8-7	+0.39901	$+0.90164\times10^{-2}$	$+0.49207\times10^{+1}$	$-0.90742\times10^{+1}$	2.45	79.31	32.4	+0.11
8-7*	+0.31148	$+0.75518\times10^{-1}$	$+0.43613\times10^{+1}$	$-0.26665\times10^{+2}$	2.31	75.80	32.8	+0.08
7-6	-0.45931	$+0.82729\times10^{-1}$	$+0.94355\times10^{+1}$	$-0.26169\times10^{+2}$	2.51	64.79	25.8	0.00
7-6*	-0.37053	+0.12116	$+0.77239\times10^{+1}$	$-0.36564\times10^{+2}$	2.20	56.99	25.9	-0.06
7-5	-0.41148	+0.11492	$+0.10236\times10^{+2}$	$-0.30506\times10^{+2}$	2.40	57.11	23.8	-0.06
7-5*	-0.33811	+0.14039	$+0.83400\times10^{+1}$	$-0.38062\times10^{+2}$	2.05	47.74	23.3	-0.14
7-4	-0.39709	+0.18023	$+0.10002\times10^{+2}$	$-0.42547\times10^{+2}$	2.35	53.99	23.0	-0.09
7-4*	-0.32481	+0.18553	$+0.78671\times10^{+1}$	$-0.45521\times10^{+2}$	1.91	39.78	20.8	-0.22
8-6	+0.96514	-0.32118×10^{-1}	$-0.40985\times10^{+1}$	$-0.20092\times10^{+1}$	3.54	122.97	34.7	+0.38
8-6*	+0.16730	+0.17796	$+0.24464\times10^{+1}$	$-0.53258\times10^{+2}$	3.11	74.27	23.9	+0.07
6-5	$-0.16239\times10^{+1}$	+0.26260	$+0.11019\times10^{+2}$	$-0.58720\times10^{+2}$	3.06	51.07	16.7	-0.11
6-5*	$-0.16233\times10^{+1}$	+0.26504	$+0.84829\times10^{+1}$	$-0.57695\times10^{+2}$	2.02	24.63	12.2	-0.38
9		$+0.21009\times10^{+1}$	$+0.39273\times10^{+1}$	$-0.60637\times10^{+2}$	3.12	64.70	20.7	0.00
8		+0.17570	$+0.56047\times10^{+1}$	$-0.51355\times10^{+2}$	4.22	86.87	20.6	+0.16

Total sum of squares about the mean = 5.71 $(^{o}C)^{2}$

Table 2. A statistical description of various regression algorithms produced for estimating atmospheric attenuation.

TABLE 3

	AVHRR & HIRS NOV 1979			AVHRR (MCSST) DEC 1981		
PAZAN SHIPS	#Bins	Bias	Scatter	#Bins	Bias	Scatter
Global	723	-0.2	0.60	795	0.4	0.50
N. Pacific	397	-0.2	0.60	376	0.4	0.50
M. Pacific	34	-0.2	0.45	41	0.3	0.55
N. Atlantic	270	-0.2	0.55	255	0.2	0.40
CLIMATOLOGY						
Global	4104	-0.7	0.85	4612	-0.1	0.85
N. Pacific	595	0.0	0.75	595	0.5	0.80
M. Pacific	894	-0.9	0.70	1056	-0.1	0.60
S. Pacific	1030	-0.7	0.95	1099	0.2	0.75
N. Atlantic	414	-0.4	0.45	420	-0.1	0.55
TRANSPAC XBT						
Global	457	-0.2	0.70	447	0.2	0.70
N. Pacific	258	-0.2	0.80	188	0.5	0.70
M. Pacific	199	-0.2	0.60	98	-0.0	0.55
FGGE BUOYS						
Global	400	-0.2	0.95			
M. Pacific	65	0.1	0.90			
S. Pacific	172	0.0	0.85			

Table 3. A comparison of November 1979 and December 1981 satellite measurements of sea surface temperatures with climatological and in situ measurements.

Figure Legends

Fig. 1. A pictorial description of the sounder principle--the physical effects that allow for cloud detection with infrared satellite sounder data.

Fig. 2. A scattergram showing the dependence of the discriminant function 8-4 upon the amount of cloud contamination in the VTPR field of view. The cloud contamination is measured by the difference between the analyzed field estimate and the VTPR measured window-channel estimate of sea surface temperature. The lettering position in the alphabet times ten indicates the frequency of occurrence.

Fig. 3. A scattergram showing the dependence of the discriminant function 8-4 upon the sea surface temperature. Only VTPR measurements that are determined to be cloudfree with the parametric classifier are included in this graph. The lettering convention is the same as in Fig. 2.

Fig. 4. A scattergram showing the amount of cloud contamination within all VTPR measurements as a function of the analyzed field estimate of sea surface temperature. The amount of cloud contamination is indicated by the difference between the analyzed field estimate and the VTPR measured window-channel estimate of sea surface temperature. The lettering convention is the same as in Fig. 2.

Fig. 5. A scattergram showing the amount of residual cloud contamination, within that set of VTPR measurements that pass the parametric classification tests, as a function of the analyzed field estimate of sea surface temperature. The amount of residual cloud contamination is indicated as in Fig. 4 and the lettering convention is the same as in Fig. 2.

Fig. 6. The standard deviation of the difference in two independent estimates of sea surface temperature as a function of the percentage of all measurements that are classified cloudfree with discriminant functions 8-4*, 8-6*, 6-5*, and 5-4* (see Table 1) as the threshold value of D is increased.

Fig. 7. Same as Fig. 6 except using discriminant functions 8-4, 8-6*, 6-5*, and 5-4* (see Table 1).

Fig. 8. The standard deviation of the difference in two measured estimates of sea surface temperature as a function of the percentage of all those measurements passing the uniformity

test, and which also are classified as cloudfree with discriminant functions 8-4, 6-5, 8-6, and 5-4 (see Table 1).

Fig. 9. The standard deviation of the difference in two measured estimates of sea surface temperature as a function of the percentage of all measurements that are classified as cloudfree with discriminant functions 8-4, 6-5, 8-6, and 5-4 (see Table 1). The external estimate of surface brightness temperature is replaced with VTPR window-channel measurements.

Fig. 10. The variance of the error in the predicted estimates of the temperature corrections, $\sigma^2_{\Delta T}$, using the indicated regression algorithms (see Table 2) as a function of the variance of the error in the VTPR window-channel brightness temperature measurements, σ^2_m, resulting from residual cloud contamination. Values of σ^2_{tot} are computed from the set of data included in the regression analysis of Section 4.3, and σ^2_{SR} is assumed to be zero.

Fig. 11. A scattergram showing the dependence of the observed values of the temperature correction upon sea surface temperature. The observed temperature correction is taken to be the difference between the NESS-derived analyzed field estiamte of sea surface temperature and the VTPR window-channel brightness temperature measurements in cloudfree scenes. The lettering convention is the same as in Fig. 2.

Fig. 12. A scattergram showing the dependence of the predicted values of the temperature correction upon sea surface temperature using the regression algorithm 8-7*. The sea surface temperature estimate is obtained from the NESS-derived analyzed field. The lettering convention is the same as in Fig. 2.

Fig. 13. The percentage of the HIRS/2 sounder data passing (failing) the discriminant function cloud test as the threshold is varied vs. the average bi-directional solar reflectance at 0.6 microns of the data passing (failing) the cloud test.

Fig. 14. The temperature difference between the sea surface temperature (SST) or the HIRS window channel (H_8) and one of the HIRS water vapor channels (H_{10} or H_{11}) as a function of total atmospheric precipitable water.

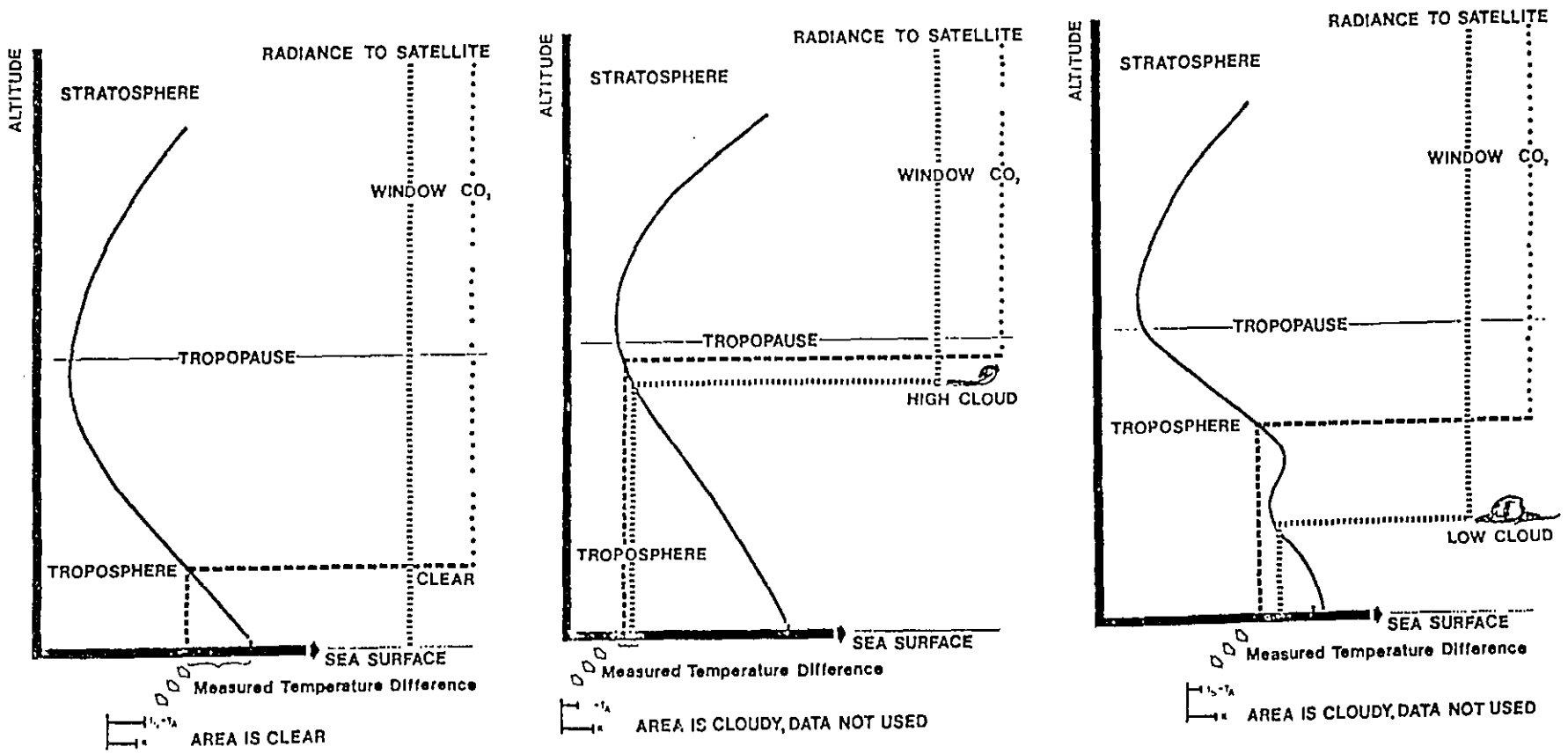

Fig. 1. A pictorial description of the sounder principle--the physical effects that allow for cloud detection with infrared satellite sounder data.

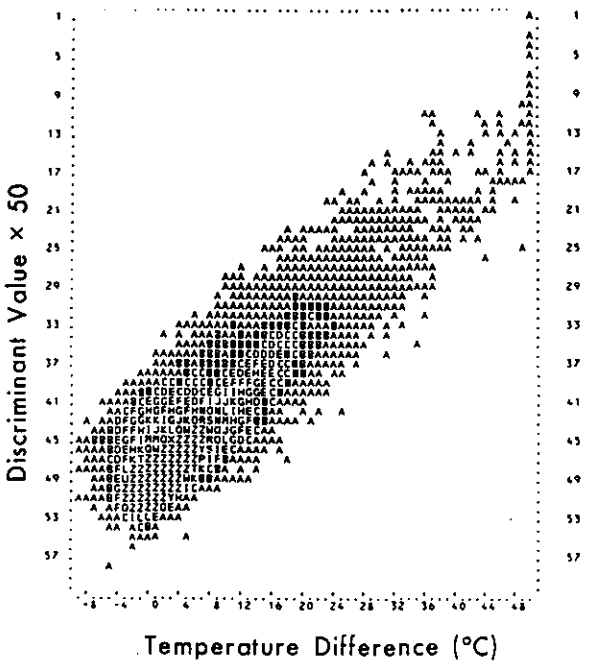

STATISTICAL BREAKDOWN INTO ORDINATE REGIONS

REGION	RANGE	SAMPLE	MEAN	SDEV	MODE	MEDIAN	SKEW
1	52- 60	3096	-0.58	1.49	-1.00	-1.00	0.28
2	51- 60	9692	-0.32	1.56	-1.00	0.0	-0.44
3	50- 60	18938	-0.06	1.66	0.0	0.0	-0.06
4	49- 60	32177	0.09	1.83	0.0	0.0	0.12
5	48- 60	33110	0.30	2.05	0.0	0.0	0.25

Fig. 2. A scattergram showing the dependence of the discriminant function 8-4 upon the amount of cloud contamination in the VTPR field of view. The cloud contamination is measured by the difference between the analyzed field estimate and the VTPR measured window-channel estimate of sea surface temperature. The lettering position in the alphabet times ten indicates the frequency of occurrence.

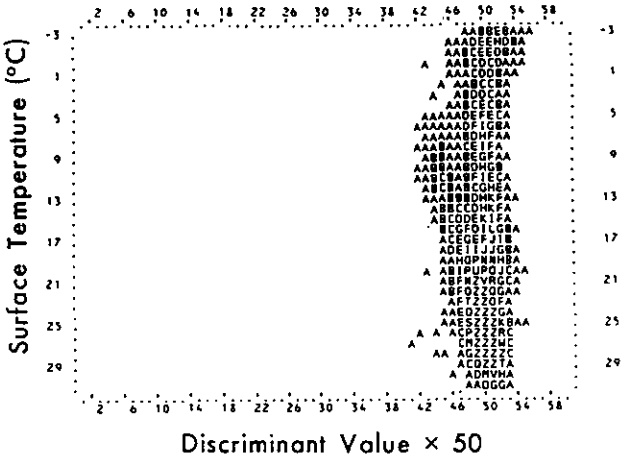

STATISTICAL BREAKDOWN INTO ORDINATE REGIONS

REGION	RANGE	SAMPLE	MEAN	SDEV	MODE	MEDIAN
1	-3- 1	824	1.02	0.03	1.04	1.02
2	2- 6	892	0.99	0.03	1.00	1.00
3	7- 11	1243	0.98	0.04	1.00	1.00
4	12- 16	1890	0.99	0.04	1.02	1.00
5	17- 21	3603	0.99	0.03	0.98	0.98
6	22- 26	8595	1.00	0.02	1.00	1.00
7	27- 31	6706	1.01	0.02	1.00	1.00
8	-3- 31	23753	1.00	0.03	1.00	1.00

Fig. 3. A scattergram showing the dependence of the discriminant function 8-4 upon the sea surface temperature. Only VTPR measurements that are determined to be cloudfree with the parametric classifier are included in this graph. The lettering convention is the same as in Fig. 2.

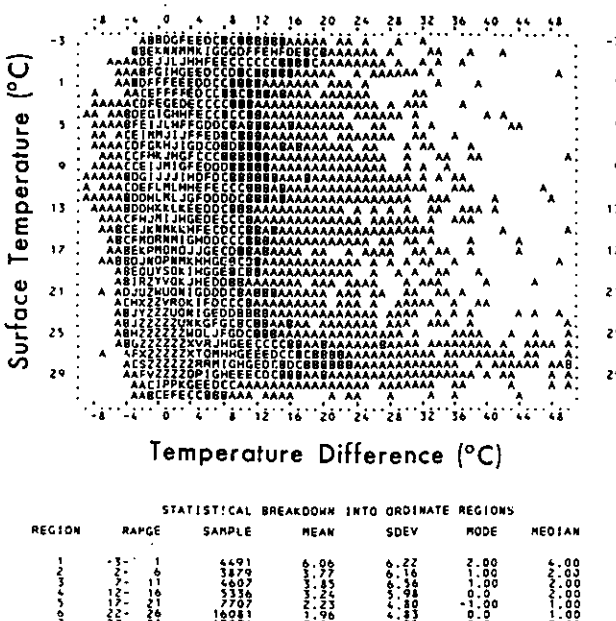

STATISTICAL BREAKDOWN INTO ORDINATE REGIONS

REGION	RANGE	SAMPLE	MEAN	SDEV	MODE	MEDIAN	SKEW
1	-3- 1	4491	6.06	6.22	2.00	4.00	0.65
2	2- 6	3879	3.77	6.16	1.00	2.00	0.45
3	7- 11	4607	3.85	6.56	1.00	2.00	0.43
4	12- 16	5336	3.25	5.98	0.0	2.00	0.54
5	17- 21	7707	2.23	5.80	-1.00	1.00	0.67
6	22- 26	16081	1.96	4.83	0.0	1.00	0.41
7	27- 31	13074	3.51	6.25	0.0	2.00	0.56
8	-3- 31	55175	3.11	5.78	0.0	1.00	0.54

Fig. 4. A scattergram showing the amount of cloud contamination within all VTPR measurements as a function of the analyzed field estimate of sea surface temperature. The amount of cloud contamination is indicated by the difference between the analyzed field estimate and the VTPR measured window-channel estimate of sea surface temperature. The lettering convention is the same as in Fig. 2.

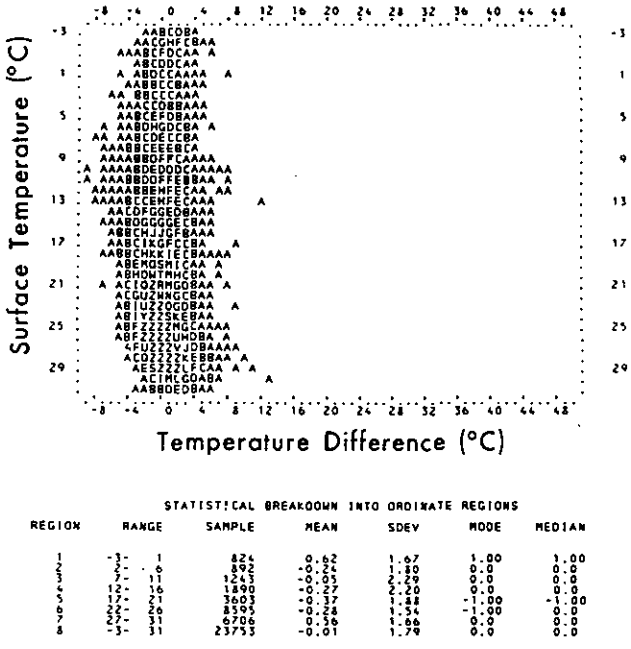

STATISTICAL BREAKDOWN INTO ORDINATE REGIONS

REGION	RANGE	SAMPLE	MEAN	SDEV	MODE	MEDIAN
1	-3- 1	824	0.62	1.67	1.00	1.00
2	2- 6	892	-0.24	1.80	0.0	0.0
3	7- 11	1243	-0.05	2.29	0.0	0.0
4	12- 16	1890	-0.27	2.20	0.0	0.0
5	17- 21	3603	-0.37	1.88	-1.00	-1.00
6	22- 26	8595	-0.28	1.54	-1.00	0.0
7	27- 31	6706	-0.56	1.66	0.0	0.0
8	-3- 31	23753	-0.01	1.79	0.0	0.0

Fig. 5. A scattergram showing the amount of residual cloud contamination, within that set of VTPR measurements that pass the parametric classification tests, as a function of the analyzed field estimate of sea surface temperature. The amount of residual cloud contamination is indicated as in Fig. 4 and the lettering convention is the same as in Fig. 2.

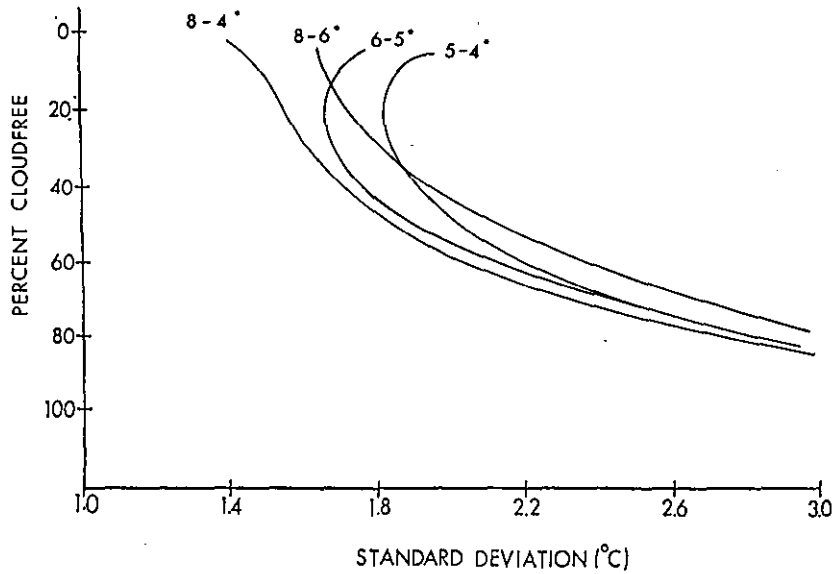

Fig. 6. The standard deviation of the difference in two independent estimates of sea surface temperature as a function of the percentage of all measurements that are classified cloudfree with discriminant functions 8-4*, 8-6*, 6-5*, and 5-4* (see Table 1) as the threshold value of D is increased.

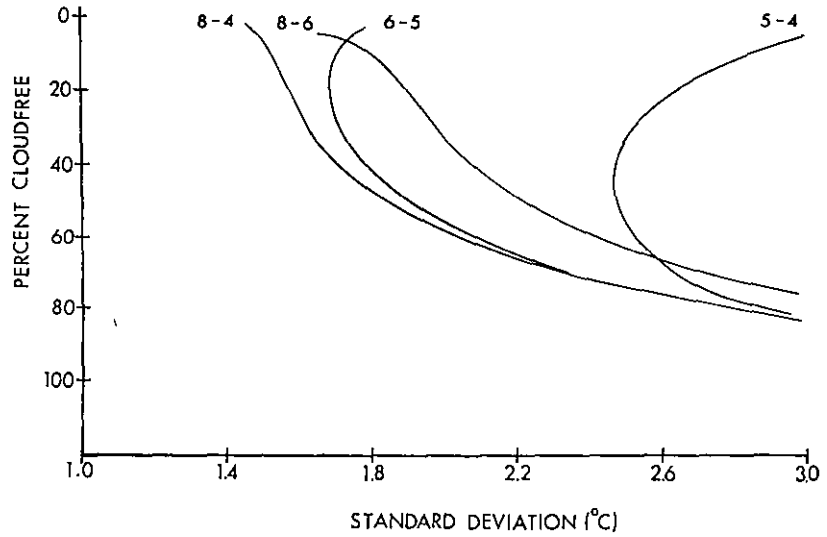

Fig. 7. Same as Fig. 6 except using discriminant functions 8-4, 8-6, 6-5, and 5-4 (see Table 1).

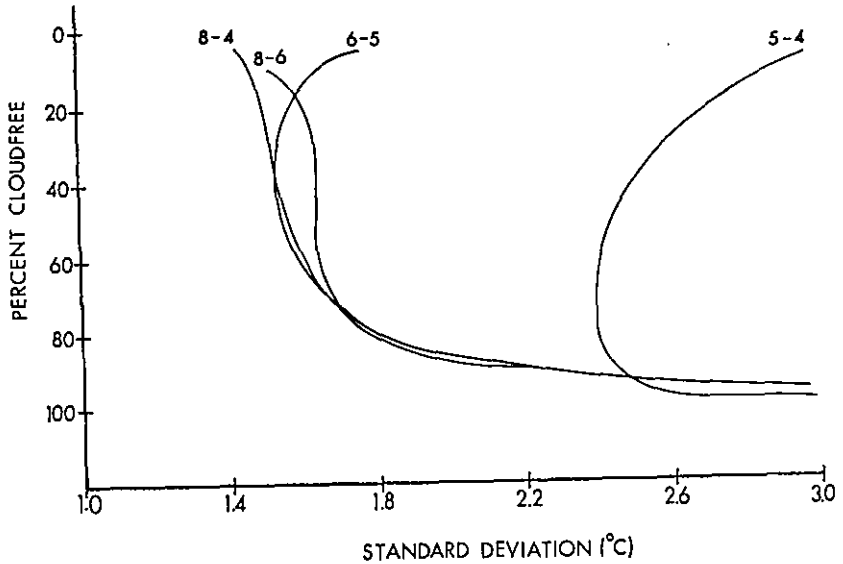

Fig. 8. The standard deviation of the difference in two measured estimates of sea surface temperature as a function of the percentage of all those measurements passing the uniformity test, and which also are classified as cloudfree with discriminant functions 8-4, 6-5, 8-6, and 5-4 (see Table 1).

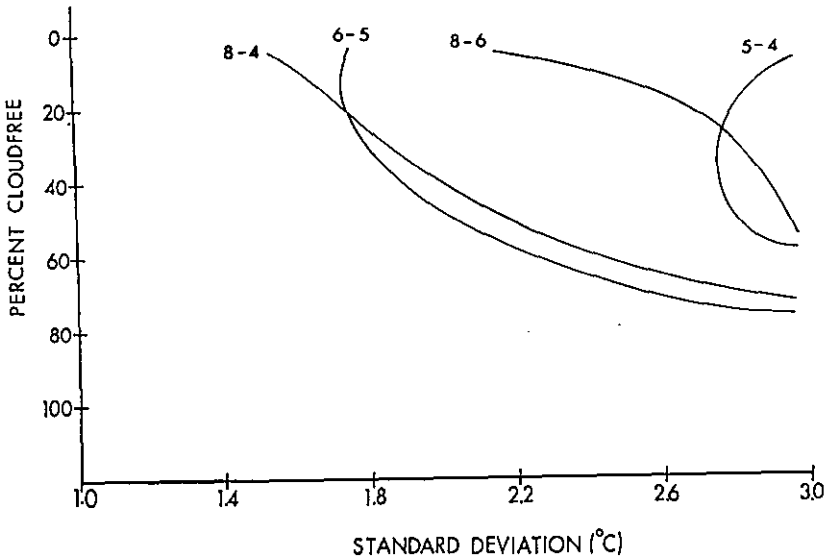

Fig. 9. The standard deviation of the difference in two measured estimates of sea surface temperature as a function of the percentage of all measurements that are classified as cloudfree with discriminant functions 8-4, 6-5, 8-6, and 5-4 (see Table 1). The external estimate of surface brightness temperature is replaced with VTPR window-channel measurements.

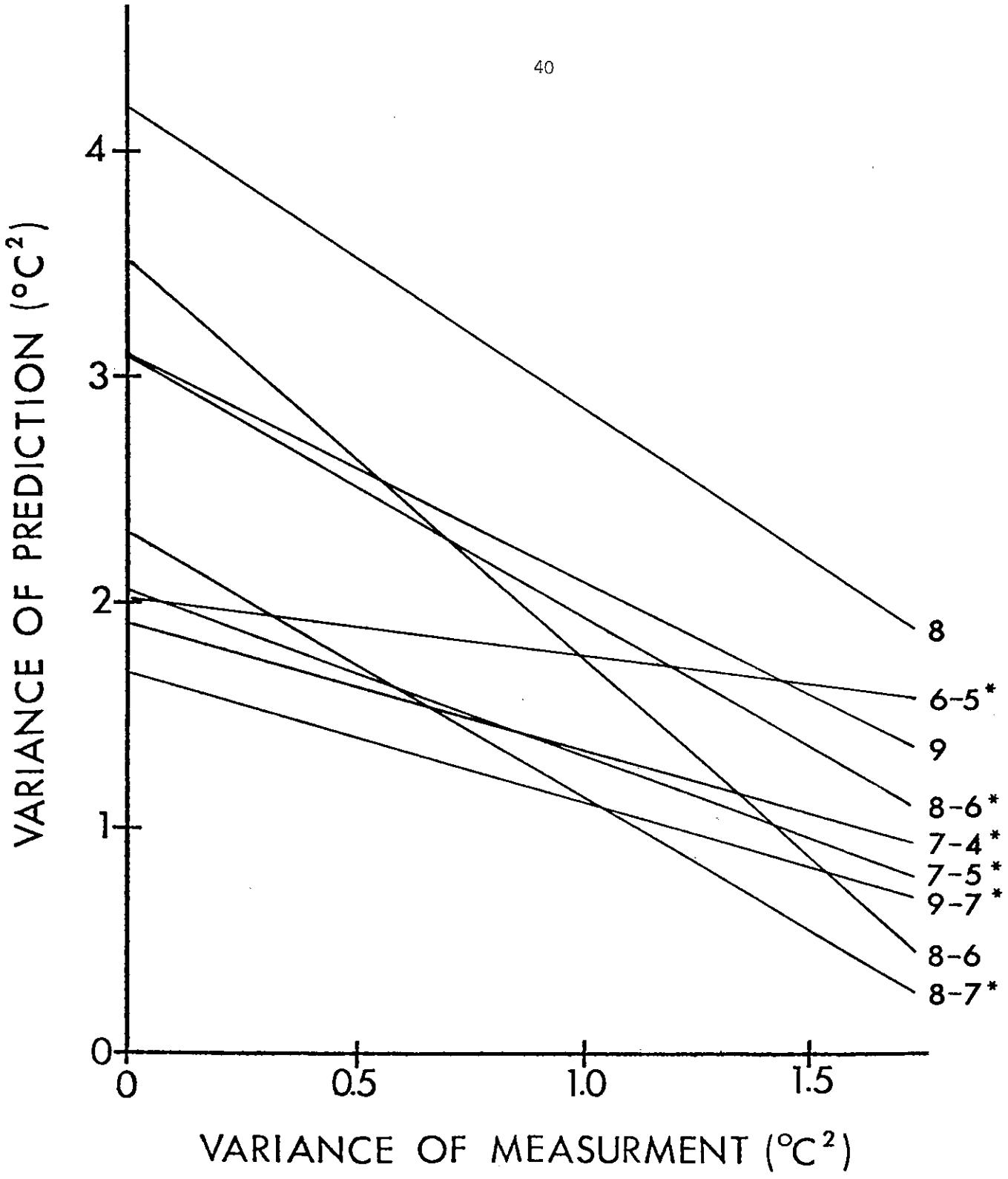

Fig. 10. The variance of the error in the predicted estimates of the temperature corrections, $\sigma^2_{\Delta T}$, using the indicated regression algorithms (see Table 2) as a function of the variance of the error in the VTPR window-channel brightness temperature measurements, σ^2_m, resulting from residual cloud contamination. Values of σ^2_{tot} are computed from the set of data included in the regression analysis of Section 4.3, and σ^2_{SR} is assumed to be zero.

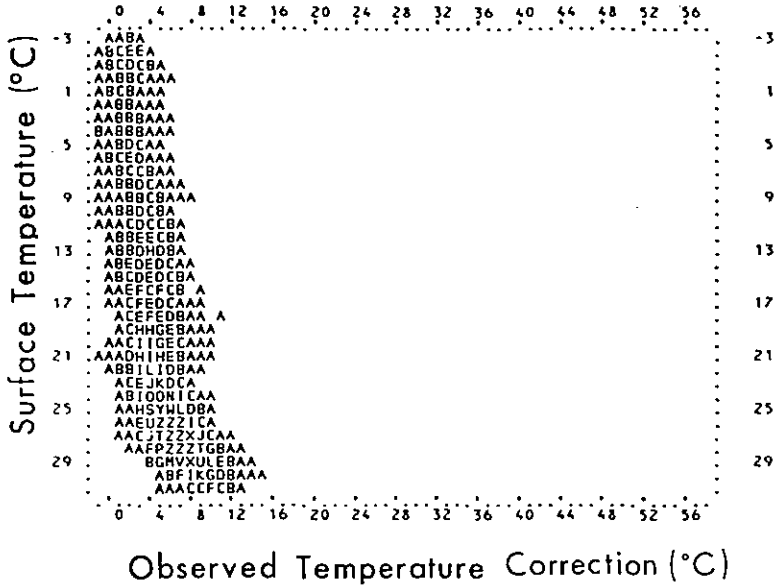

STATISTICAL BREAKDOWN INTO ORDINATE REGIONS

REGION	RANGE	SAMPLE	MEAN	SDEV	MODE	MEDIAN	SKEW
1	-3- 1	465	1.89	1.35	2.00	2.00	-0.08
2	2- 6	429	1.93	1.50	2.00	2.00	-0.05
3	7- 11	556	3.05	1.56	3.00	3.00	0.03
4	12- 16	1017	3.77	1.65	4.00	4.00	-0.14
5	17- 21	1472	4.29	1.67	4.00	4.00	0.17
6	22- 26	3607	5.19	1.50	5.00	5.00	0.13
7	27- 31	4372	7.40	1.28	7.00	7.00	0.22
8	-3- 31	11918	5.42	2.39	5.00	5.00	0.18

Fig. 11. A scattergram showing the dependence of the observed values of the temperature correction upon sea surface temperature. The observed temperature correction is taken to be the difference between the NESS-derived analyzed field estiamte of sea surface temperature and the VTPR window-channel brightness temperature measurements in cloudfree scenes. The lettering convention is the same as in Fig. 2.

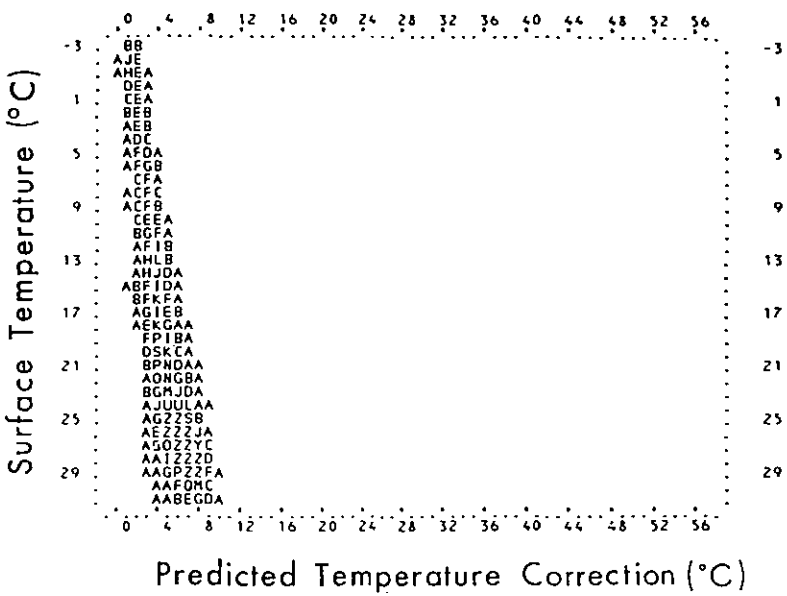

STATISTICAL BREAKDOWN INTO ORDINATE REGIONS

REGION	RANGE	SAMPLE	MEAN	SDEV	MODE	MEDIAN	SKEW
1	-3- 1	465	1.46	0.56	1.00	1.00	0.82
2	2- 6	429	2.31	0.67	2.00	2.00	0.47
3	7- 11	556	3.04	0.75	3.00	3.00	0.06
4	12- 16	1017	3.78	0.81	4.00	4.00	-0.27
5	17- 21	1472	4.30	0.85	4.00	4.00	0.35
6	22- 26	3607	5.70	1.05	6.00	6.00	-0.29
7	27- 31	4372	6.96	1.03	7.00	7.00	-0.04
8	-3- 31	11918	5.41	1.85	7.00	6.00	-0.86

Fig. 12. A scattergram showing the dependence of the predicted values of the temperature correction upon sea surface temperature using the regression algorithm 8-7*. The sea surface temperature estimate is obtained from the NESS-derived analyzed field. The lettering convention is the same as in Fig. 2.

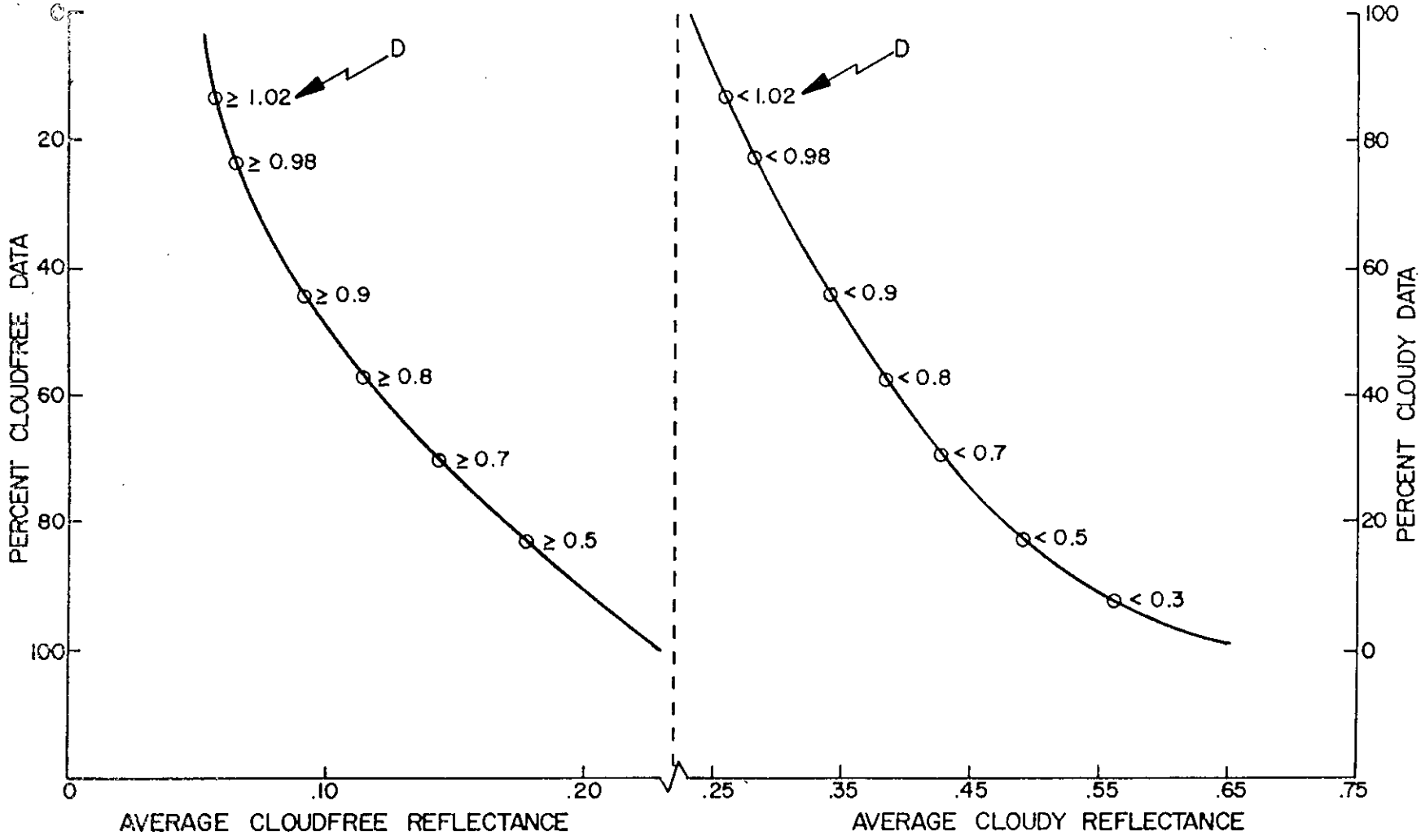

Fig. 13. The percentage of the HIRS/2 sounder data passing (failing) the discriminant function cloud test as the threshold is varied vs. the average bi-directional solar reflectance at 0.6 microns of the data passing (failing) the cloud test.

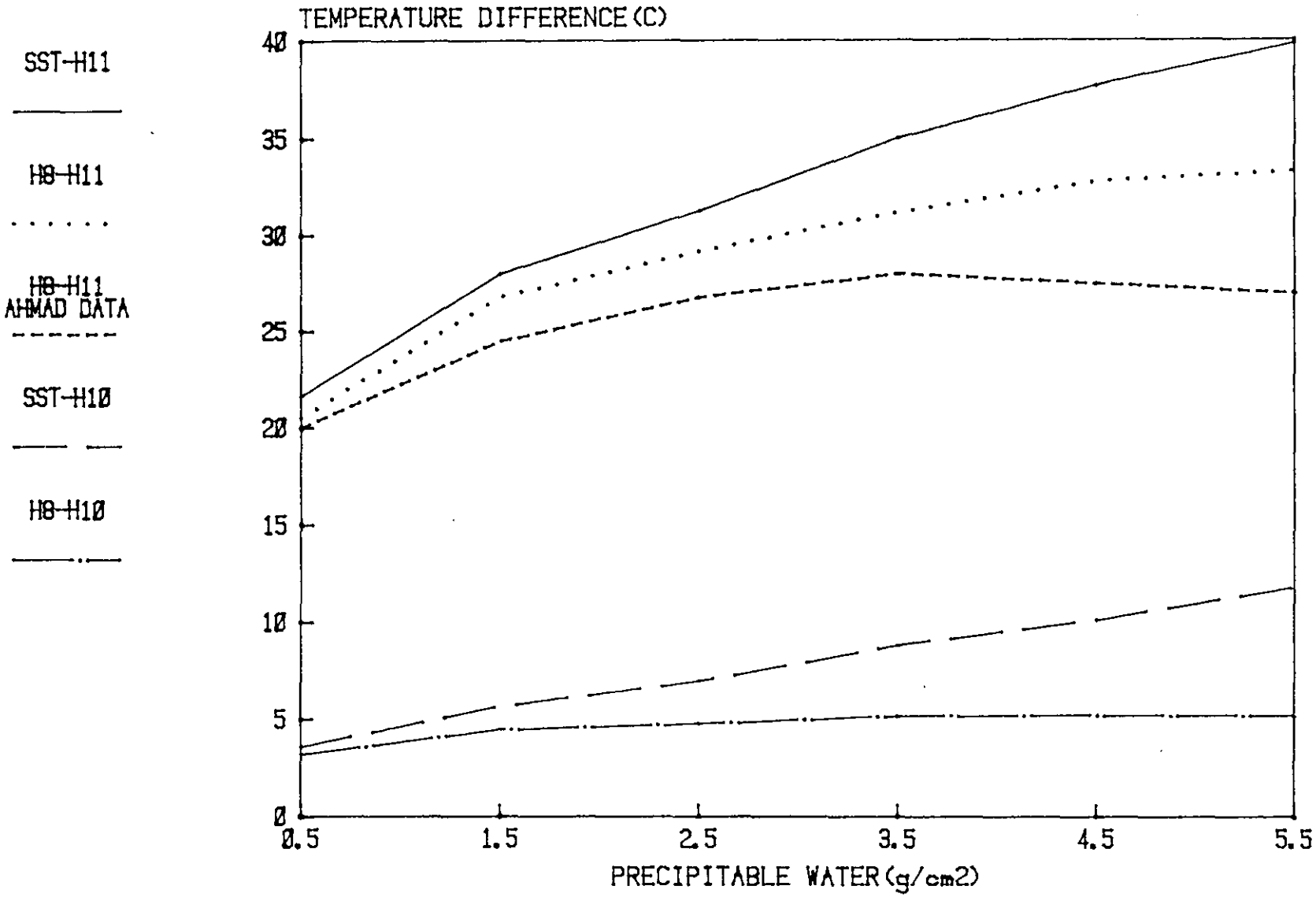

Fig. 14. The temperature difference between the sea surface temperature (SST) or the HIRS window channel (H_8) and one of the HIRS water vapor channels (H_{10} or H_{11}) as a function of total atmospheric precipitable water.

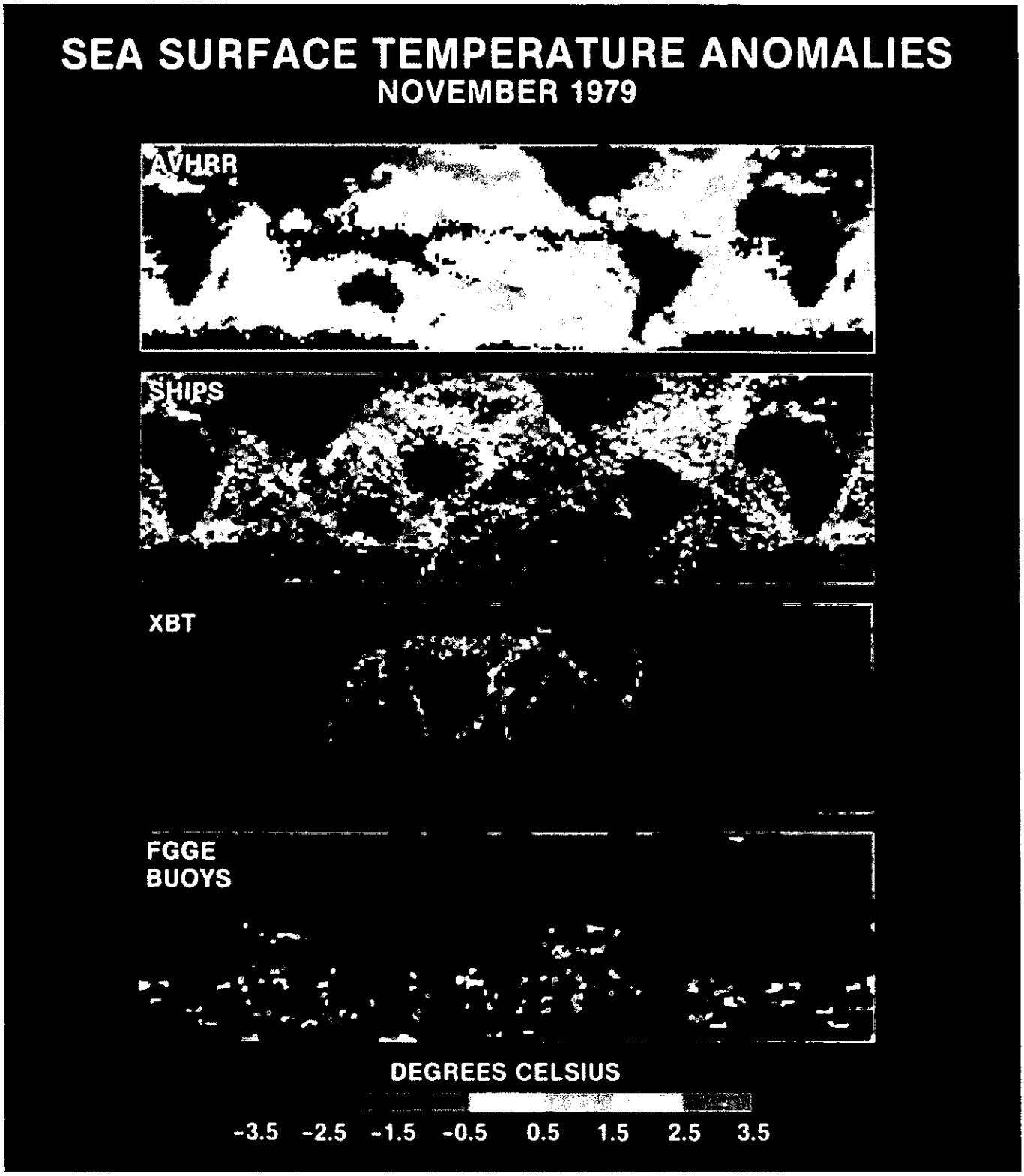

Figure 15. SST anomalies for November 1979: (a) AVHRR, (b) ships, (c) XBT's, (d) FGGE buoys.

APPENDIX A Historical Record of Significant Events Affecting the TIROS-N series Satellites, and Heat Budget SST Products

10/13/78
Launch of the TIROS-N spacecraft, the prototype for the third generation of polar-orbiting operational environmental satellites. The TIROS-N series replaces the ITOS series (i.e., NOAA-1 to NOAA-5).

12/4/78
Begin calculation and archive of sea surface temperatures (SST's) derived from TIROS-N data. Equivalent black body temperatures are obtained from the 11 micrometer channel of the AVHRR using the truncated normal technique on targets of 11 by 11 samples of 4 km resolution global area coverage (GAC) data. Gross cloud detection requires that the AVHRR 11 micrometer channel and the HIRS/2 channel 8 (H8) (an 11 micrometer channel) not differ by more than 2°C after correction for the average difference between the two channels (average difference is 1°C with the H8 being smaller than the AVHRR 11 micrometer channel). Also the difference between H8 and H7 must exceed 17°C. Primary cloud detection is performed with a discriminant classifier determined by regression using data from November 15 and 16, 1978. Coefficients of the discriminant classifier were determined by a global regression using the gross cloud tests to determine the clear targets. The discriminant functions are as follows:
Type 129 (AVHRR and HIRS/2 coincident data available)
D= -0.9963863E-02 (Climatology - 290)
+0.2248869E-01 (H8-H5)
+0.2171421E-02 (H10-H11)
-0.1852268E+00 (Secant of the Zenith Angle -1)

Type 130 (AVHRR Data Only)
D= 0.2080572E-01 (AVHRR 11 Micrometer Channel - Climatolgy)
+0.3665414E-02 (Climatology-290)
+0.4795260E-01 (Secant of the Zenith Angle -1)

All values in the discriminant equation are in degrees K. Climatology is the nearest 1° latitude/longitude gridpoint climatological SST value for the month. The value of D must be between 0.98 and 1.20 for the target to be classified as clear. Clear 11 micrometer equivalent black body temperatures are then corrected for the effects of atmospheric attenuation by using a regression equation derived from data for November 15 and 16, 1978.

Using Northern Hemisphere Climatology for the ground truth data, the atmospheric attenuation correction equations are as follows:

Type 129 (Coincident AVHRR and HIRS/2 Data)
DELTA T = -0.1498916E+02
+0.4699983E-01 (100 km Field SST)
+0.1256545E+00 (100 km Field SST - H11)
+0.1047428E+01 (Secant of the Zenith Angle -1)

Type 130 (AVHRR Only)
DELTA T = -0.3155946E+02
+0.1177870E+00 (100 km Field SST)
+0.1686770E+01 (Secant of the Zenith Angle -1)

The 100 km and 50 km fields were initialized with December climatology.

1/1/79
End-of-Year problems caused some directory errors in the 7-day observation archive file for this week.

2/1/79
Observations in the tropics are generally over 1 degree C too low. The cause is residual cloud contamination, and it was decided to incorporate a neighbor check to eliminate cloud contaminated observations. Began neighbor check procedure for all observations between 20 degrees north and south. Each observation is compared with an average temperature of surrounding observations. The observation is rejected if it differs from the average by more than 1 degree C.

2/28/79
Formal end of ITOS operation. TIROS-N is designated as the operational satellite. The TIROS-N SST archive, however, will be maintained beginning 1/1/79.

5/9/79
Terminated neighbor check procedure in the tropics. Substituted stricter discriminant function limits when the SST is above 297 degrees K. The stricter limits are 1.02 to 1.20.

6/10/79
Repaired a logic problem in the SST retrieval module which prevented the retrieval of SST's in the vicinity of the Date Line.

10/13/79
Launch of NOAA-A, designated NOAA-6 in orbit. This is the second satellite in the TIROS-N series.

11/1/79
Beginning in mid April and continuing until Fall, accuracy above 30 degrees North latitude is poor. Current regression equations overcorrect for atmospheric attenuation in the high latitudes in the summer hemisphere. Also, SST's in the vicinity of the northwest coast of Africa are too high.

1/1/80
Heat budget analysis scheme changed. Mercator fields are now produced from the polar-stereographic fields. During 1979, the stereographic fields were derived from the mercator fields.

1/20/80
An on-board computer failure terminates TIROS-N data reception.

1/22/80
The NOAA-6 satellite, the second satellite in the TIROS-N series, is designated as the operational satellite.

1/25/80
Began calculating SST's from NOAA-6 satellite. Regression coefficients were calculated from January 22 and 23 data using Northern Hemisphere January climatology as ground truth. Gross cloud detection tests are the same as TIROS-N. Discriminant classifier is as follows:

Type 129 (Coincident AVHRR and HIRS/2)
D= -0.68785E-02 (Climatology - 290)
+0.23452E-01 (H8-H5)
+0.16013E-02 (H10-H11)
-0.17712E+00 (Secant of the Zenith Angle -1)

Type 130 (AVHRR only) Not Used

All temperatures are in degrees K. Climatology is the nearest 1 degree latitude/longitude gridpoint climatology value for the month.

Atmospheric attenuation correction equation was obtained by regression using Northern hemisphere climatology for January as ground truth. The atmospheric attenuation correction equation is:

Type 129 (Coincident AVHRR and HIRS/2)
DELTA T = -0.19640E-02 + 0.60360E-01 (100 km Field SST)
+.15323E+00 (100 km Field SST - H11)
+0.21380E+01 (Secant of the Zenith Angle -1)

Type 130 (AVHRR only) Not Used

1/28/80
Observation accuracy has been degrading during the last few days. The problem has been traced to the regression equation.

1/29/80
Changed regression for atmospheric attenuation correction. Ground truth was changed to the 100 km field analysis temperature in the Northern hemisphere for 1/20/80. The new regression equation is as follows (Discriminant function was not changed):

Type 129 (Coincident AVHRR and HIRS/2)
DELTA T = -0.2067618E+02
+0.6683129E-01 (100 km SST)
+0.1394463E+00 (100 km SST - H11)
+0.2606292E+01 (Secant of the Zenith Angle -1)

4/29/80
A slight increase in the IR channel space view noise has caused the loss of up to 16 percent of the data since 4/11/80. The upper limit of the space view variance was increased from 1 to 2 counts to accept the noisier data.

4/30/80
The threshold of the gross cloud detection test (the difference between HIRS channel 8 (the window channel) and channel 7 (the lower tropospheric channel), was decreased from 17 degrees C to 15 degrees. This essentially relaxes the cloud test at high latitudes where it has been too restrictive (especially with the NOAA-6 data).

5/2/80
Version 2.0 of the Heat Budget data reduction module was implemented. This version allows correct day/night decision in the creation of flux fields using data from a morning satellite.

8/5/80
Implemented new cloud descrimination coefficients based on data passing the 15 degree gross cloud test. The descriminant equation is now:

D= -0.78161E-02 (Climatology - 290)
+0.22398E-01 (H8-H5)
+0.41897E-02 (H10-H11)
-0.15995E+00 (Secant Satellite Zenith Angle -1)

The minimum threshold for D above 290 degrees K surface temperature is 1.03, for the rest of the Southern hemisphere it is 0.99, for the rest of the Northern hemisphere it is 0.98.

8/6/80
Implemented a bias correction to correct for the warm bias in high latitudes of the summer hemisphere. The correction C is calculated as follows and added to the calculated SST. C = Table Value - (H8-H7) where H8 and H7 are the temperatures sensed in HIRS channel 8 (the window channel) and 7 (the lower tropospheric channel). This correction is thus proportional to the lapse rate in the lower troposphere. The table value is a function of the calculated SST before correction. The table is as follows:

SST	Bias Correction	SST	Bias Correction	SST	Bias Correction
270	14.5	280	16.6	290	19.3
271	14.6	281	16.9	291	19.4
272	14.8	282	17.0	292	19.5
273	14.9	283	17.3	293	19.6
274	15.1	284	17.4	294	20.0
275	15.4	285	17.8	295	20.5
276	15.6	286	18.4	296	20.8
277	15.8	287	18.9	297	21.1
278	16.0	288	19.0	298	21.3
279	16.3	289	19.1	299	21.0

8/26/80
It was discovered that the maximum atmospheric correction allowed is 8 degrees C. Areas in the western tropical Pacific regularly have corrections greater than 8 degrees C. Corrections as high as 15 degrees will be allowed for generating a regression tape used to calculate the atmospheric correction coefficients. The limit will continue to be 8 degrees in the operational processing of SST.

1/20/80
An undetected disk I/O error on Thursday, November 20 resulted in a heat budget observation dated July 28, 1984. Daytime longwave flux and absorbed solar energy analyzed fields were set up for the erroneous date, interfering with the daily field analysis for the next three days. To solve the problem, the field files were initialized. Nighttime longwave flux fields were not affected by the erroneous observation; however, 10 hours of nighttime data were lost in the field initialization.

1/31/80
Eight hours of data were lost due to an incorrect manual entry of the date on the preprocessing computer.

1/24/81
The heat budget absorbed field was incorrect from 1/17/81 to 1/24/81 due to a bad program load module.

1/26/81
An error in the IBM 360 CPU resulted in loss of the 100km SST analyzed field. The field for 1/25/81 was reloaded and the field generation program was rerun. An incorrect data card did not allow any inclusion in this field of data from 1/25/81.

2/6/81
The heat budget product network was run after midnight resulting in the calculation of a heat budget analyzed field for the wrong date. The backup program was run too late. The field for 2/4/81 was lost.

8/19/81
The operational spacecraft was switched from NOAA-6 to NOAA-7. Three weeks of operational parallel testing were conducted before the switch. Regression equations were calculated using data collected between 7/21/81 and 7/23/81. Atmospheric attenuation regression coefficients were calculated using the NOAA-6 satellite 100km analyzed field as ground truth. The gross cloud tests remain identical to NOAA-6. The NOAA-7 cloud discriminant function is:

D= -.005565330 (Climatological SST - 290)
+.02280071 (H8-H5)
+.002125098 (H10-H11)
-.1565646 (Secant of the Zenith Angle - 1)

The atmospheric attenuation equation for NOAA-7 is:

DELTA T= -13.37065
+.03274177 (100 km analyzed field SST)
+0.2143435 (100 km analyzed field SST - H11)
+0.9215280 (Secant of the Zenith Angle - 1)

The bias correction was also changed for NOAA-7 and is being applied only in the Northern hemisphere. The bias values are now:

SST	Bias Correction	SST	Bias Correction	SST	Bias Correction
270	14.5	280	16.6	290	19.2
271	14.6	281	16.9	291	19.4
272	14.8	282	17.0	292	19.4
273	14.9	283	17.3	293	19.4
274	15.1	284	17.4	294	19.6
275	15.4	285	18.6	295	20.5
276	15.6	286	19.3	296	20.7
277	15.8	287	19.7	297	21.9
278	16.0	288	19.7	298	21.2
279	16.3	289	19.3	299	20.9

8/25/81
Most of the observations for 8/24/81 and 8/25/81 had to be purged. A faulty disk pack resulted in erroneous calibration coefficients and thus erroneous observations. The NESDIS archive will not contain any erroneous data.

9/17/81
Calibration coefficients are erroneous for data from 0000Z to 2119Z. Bad data was purged from the archive.

9/28/81
Calibration coefficients are erroneous for data from 0018Z to 1407Z. Bad data was purged from the archive.

11/17/81
The operational technique for calculating sea surface temperatures was changed to a multichannel technique. Separate algorithms are used for day and night observations. The algorithm is denoted by the observation type. Type 151 is daytime operational observations derived from the AVHRR instrument alone. Type 152 is nighttime AVHRR operational observations. Daytime sea surface temperatures are calculated with a split-window quadratic equation:

$SST=1.046(T4) + 1.666(T4-T5) + 0.528(T4-T5)\ (T4-T5) - 286.48$

Where SST = sea surface temperature in Centigrade.
T4=11 Micrometer AVHRR Channel temperature in Kelvin
T5=12 Micrometer AVHRR Channel temperature in Kelvin

Nighttime sea surface temperatures are calculated with a triple window equation:

$SST= 1.0224(T4) +1.00144(T3-T5) -278.515$

where terms are the same as the daytime equation and T3=3.7 micrometer AVHRR channel temperature in Kelvin. Sea surface temperatures are calculated from 8km resolution areas spaced about 25km apart from all regions of the global ocean and the larger inland seas such as the Caspian sea.

11/24/81
Changed precision of AVHRR daytime operational equation. New equation is as follows:

$SST= 1.0460(T4) + 1.6662(T4-T5) + 0.5285(T4-T5)\ (T4-T5) - 286.4595$

11/27/81
A system error resulted in no SST observations for 11/25/81.

11/30/81
The first monthly mean charts containing multichannel observations are dated 11/30. These charts are derived partly from SSTs calculated with the former operational technique and partly from the multichannel observations.

12/2/81
Implemented a low stratus nighttime cloud test. T4-T3 is not allowed to be greater than 0.7 degrees Centigrade.

12/31/81
Produced the first monthly mean charts derived solely from multichannel data.

2/23/82
Changed daytime operational equation to a split-window linear equation:

$SST= 1.0351(T4) + 3.046(T4-T5) - 283.9267$

Began calculating 8km density observations off Peru, in Gulf of Mexico, and off the East Coast of the United States.

APPENDIX B

FACTORS AFFECTING THE ACCURACY OF SATELLITE-DERIVED SEA SURFACE TEMPERATURES

About a year ago, the factors affecting the accuracy of satellite SST were detailed in Appendix C of a memo entitled, "Report on the Current Status of the Operational AVHRR Quantitative Products System" (Pichel and Brower, November 27, 1979). Investigations have continued during the year since that report was circulated, mostly in conjunction with the SST Improvement Contract with SASC. The SASC Contract is now complete and it is time to update last year's report with the findings obtained during the last twelve months. This report supplements the final contract report entitled, "Estimation of Sea Surface Temperature from TIROS-N/NOAA-6 Spacecrafts" (Ahmad, September 30, 1980).

Our understanding of the factors affecting the accuracy of satellite SST has advanced considerably in the past year. The major factors affecting the accuracy (in order of importance) are:

A. Atmospheric Attenuation Correction
B. Cloud Detection
C. Regression and Verification Procedures
D. Measurement of Equivalent Black-Body Temperature
E. Calibration Procedures
F. Field Analysis Procedures

The following sections detail our understanding of these major factors and some minor factors affecting the accuracy of satellite SST.

The simulated data upon which a number of the conclusions are based were provided through the efforts of Z. Ahmad of SASC.

A. Atmospheric Attenuation Correction

The current regression equation used for atmospheric attenuation correction is:

$$\Delta T = -20.68 + .067\ (T_{sst}) + .14\ (T_{sst} - H_{11}) + 2.61\ (\sec \Theta - 1)$$

Where ΔT = the atmospheric attenuation correction (^{o}K)

T_{sst} = analyzed field SST (^{o}K)

H_{11} = HIRS Channel 11 temperature (^{o}K)

Θ = local zenith angle

1. HIRS Channel 11

In the regression equation, HIRS channel 11 is useful only to the extent that it broadly catagorizes the type of atmosphere (i.e. tropical or polar) but provides little skill in measuring the variation in moisture within a particular type of atmosphere. Channel 11 peaks too high in the atmosphere to track low-altitude moisture variations. The same total amount of moisture distributed in different ways with height will produce different values of H_{11}, and the variations in H_{11} are not necessarily correlated with the total amount of moisture or the total attenuation. The current regression coefficients give atmospheric corrections applicable to a mean atmosphere, but fail to predict ΔT correctly for atmospheres where the moisture distribution differs from the mean. The ΔT contribution by the $T_{sst} - H_{11}$ term in the current algorithm is less than 45% (contributions range between 2^{o} C and 4^{o} C) of the total ΔT. The remaining ΔT is an empirical function of temperature; thus, the current algorithm is highly empirical and dependent on a surface temperature estimate rather than on atmospheric measurements. In fact, for mean atmospheres, other HIRS channels add almost as much skill as H_{11} in predicting ΔT. Mean atmospheric conditions occur over 60% to 70% of the ocean in clear cases. The other 30% to 40% of the clear cases produce incorrect ΔT estimates.

2. Failure in Moist Atmospheres

The difference between a measure of surface temperature (i.e., analyzed field SST, H_8, or AVHRR Channel 4) and H_{11} is not in itself a measure of the amount of moisture in the atmosphere, especially at high values of total precipitable water (Figure 14) (Ahmad Data). above approximately 3 gm/cm^2 ppt H_2O, the $H_8 - H_{11}$ difference becomes constant, whereas the expected ΔT continues to increase at a rate of 1.8^{o}C/gm/cm^2. HIRS channel 11, therefore, does not predict ΔT at mixing ratios much above 3 gm/cm^2.

3. Need for Atmospheric Temperature Information

There is evidence that the current regression equation produces error patterns that are correlated with atmospheric temperature. The bias correction makes use of this effect by correcting the ΔT values by using the $H_8 - H_7$ difference (i.e., the difference between the window and the lower tropospheric channel of HIRS). Algorithms which use information on the distribution of atmospheric temperature from HIRS have demonstrated improved accuracy over the operational algorithm. The ideal algorithm would be one that modeled the temperature and moisture distribution in the total atmosphere. In coastal regions with offshore flows at low and mid levels, the current model always overestimates ΔT because warm dry air exists. H_{11} indicates a small but significant correction on top of a large empirical correction (given by T_{sst}) to an equivalent black-body temperature which is already very close to the actual surface temperature.

4. Use of Analyzed Field SST

The current regression equation is dependent on the satellite SST analyzed field (T_{sst}) which (geographically biased) can be in error by 3^{o}C to 4^{o}C, and which in some regions has not been updated in months. Use of the black-body temperature in place of the analyzed field SST results in a more stable ΔT with less standard deviation, and smaller errors in the tropics.

5. Zenith Angle Term

The single zenith angle term (sec Θ-1) in the present regression equation may not be adequate if other HIRS channels are employed, since each channel has a different dependence on slant path . Slant path corrections are now applied as a constant for all temperature and moisture combinations. This may not be the best procedure since the slant path attenuation is actually a function of temperature and moisture structure. As an illustration, consider a completely dry atmosphere. For this case, the secant term would add nothing to ΔT at $\Theta = 0$ and 0.9^{o} C to ΔT at $\Theta = 42^{o}$, resulting in overcorrection at higher zenith angles.

6. Possible Use of Channel 10

HIRS channel 10 could be used in place of channel 11 to make the algorithm more responsive to low-altitude moisture since channel 10 peaks lower in the atmosphere. Polarization errors in channel 10 seem to be self-compensating and no zenith angle dependence is indicated when channel 10 is used for atmospheric attenuation correction.

7. Maximum Atmospheric Correction is Too Low

There is a cutoff on the maximum allowed atmospheric attenuation correction. This cutoff is currently set at 8^{o} C. In the western tropical Pacific, corrections are often as high as 10^{o} C; thus, this cutoff is limiting observations in some tropical regions. The cutoff should be raised to 10^{o} C.

8. Need for Daytime and Nighttime Algorithms

Channels H_7, H_{11}, H_5, and H_6 do respond significantly (3^{o}c) to diurnal changes; thus, different algorithms or coefficients for day and night may be required.

B. Cloud Detection

Currently there are three cloud tests (in addition to a cloud filter inherent in the truncated-normal measurement technique). These are:

1. $H_8 - H_7 \geq 15^{o}$ C
2. $T_{bb} - H_8 \leq 2^{o}$ C

Parametric Classifier

3. $D = -.0078\ (CLIMO - 290) + .0224\ (H_8 - H_5) + 0.00419\ (H_{10} - H_{11}) - .159\ (SEC\ \Theta - 1)$

Discriminant Classifier

where

H_8, H_7, H_5, H_{10}, H_{11} are HIRS channel 8, 7, 5, 10, 11 temperatures (^oK) respectively

T_{bb} is the equivalent black-body temperature (^oK) obtained from the AVHRR 11 μm channel by the truncated-normal measurement technique

CLIMO is the climatological temperature (^oK)

θ is the local zenith angle

D is a value which must fall within limits which are determined to minimize the amount of cloud contamination. Non-tropical limits are .98 and 1.20. Tropical limits are 1.02 and 1.20.

1. Inflexibility of 15^o C Test

In the first test of the parametric classifier, the same threshold (i.e. 15^o C) is used regardless of the location of the observation. The average difference between H_8 and H_7 varies with latitude (greater in the tropics, less in the polar regions) ; thus, the sensitivity of this test is a function of latitude. This test tends to be restrictive in high latitudes and permissive in low latitudes. Many cloud contaminated tropical retrievals are designated as clear and are used in the regression procedure which calculates the coefficients for the discriminant classifier. It has been necessary to make the limits on D more restrictive in the tropics to prevent large numbers of cloudy observations. This parametric classifier test should be a function of latitude, temperature, or solar zenith angle. There may be diurnal changes in sensitivity of this test as well.

2. Differences Between Window Channels of HIRS and AVHRR

In regard to the second parametric classifier test which compares the 11 μm window channels of the AVHRR and the HIRS/2, the two channels can differ by more than 2^o C in "clear" cases as a function of sub-resolution cloudiness (to which the HIRS is more susceptible) and moisture (to which the AVHRR is more susceptible). This test is often rejecting data for reasons other than cloudiness. In some tropical atmospheres the difference is inconsistent, and may vary between night and day. H_8 is frequently larger than T_{bb} in nighttime tropical atmospheres. The spectral responses of the window channels of the two instruments are quite different

3. Variable Sensitivity of Discriminant Classifier

The current cloud detection discriminant classifier regression equation is sensitive in high latitudes and very permissive in low latitudes. In response to this behavior, the limits of acceptance for clear retrievals have had to be altered for regions with temperatures above 26° C. The stricter limits above 26° C severely limit retrievals in the tropics.

The term $H_8 - H_5$ in the discriminant classifier varies substantially between summer and winter, making this cloud test more restrictive in summer than in winter , resulting in loss of SST observations in high latitudes in summer and poor field contours.

4. Use of a Single Zenith Angle Term

The single additive zenith angle correction term in the discriminant classifier may not adequately correct for slant path effects since each HIRS/2 channel is affected differently by increasing atmospheric path length. Specifically, the limb-darkening correction for H_5 is larger than given by the sec θ-1 term of the present discriminant classifier.

5. Lack of Target Rejection Statistics

Improvement of cloud-detection thresholds would be aided by statistics on the number of targets failing each specific cloud test as a function of geographic region.

C. Regression and Verification Procedures

The current regression procedure is a simple multi-linear regression using either climatology or the satellite SST analyzed field as ground truth. The satellite observations are verified using a large sample of ship observations obtained from NMC. The ship observations are quality controlled only by a gross comparison with climatology (ship observations must not differ from climatology by more than 7°C). The last three days of ship data are compared with the last 24 hours of satellite data and statistics are generated for all pairs of satellite and ship measurements separated by 100 km or less.

1. Use of One Equation for the Entire World

The current regression procedure utilizes one equation for the entire world. The equation fits the mean case quite well, but cannot be optimized for atmospheric conditions different from the mean. The regression procedure is optimized to give the most consistent accuracy in subtropical high pressure regions in the winter hemisphere (since this is where most satellite observations occur). There is no attempt to evenly weight different atmospheric regions when regression coefficients are calculated.

2. Inaccurate Ground Truth in Regression

The regression coefficient generation procedure can only use climatology or the satellite SST analyzed field for sea truth. If these are incorrect, the regression is incorrect. Climatology can differ by up to 4°C

from current sea truth. The Southern Hemisphere Climatology is particularly unreliable. Accurate ship data must be used as sea-truth in the regression procedure, if there is to be any hope of improvement.

3. Lack of an Automated System for Regression Generation

Regression coefficients can be calculated only using satellite data from a small sample of data (any two consecutive days). This makes it difficult to minimize seasonal effects. Generation and verification of regression coefficients takes at least a week and requires substantial manual intervention. The implementation of improved coefficients is, thus, delayed.

4. Quality of "Sea-Truth" Data

The quality of the ship data used as sea-truth in verification is very poor. Screening the ships against climatology helps some, but the variance of the ship data is still higher than that of the satellite data. Neighbor tests on the current ship data may help some, but further improvements in the ship data set are questionable. It is recommended that the total ship file be used only for bias analysis in long term trends. There is very little information to be found in standard deviation or RMS error statistics except when comparing satellite observations obtained by different algorithms. A separate verification should be done using only the fixed and drifting buoys, weather ships, and XBT's. If necessary, this new set of highly accurate sea-truth data should be hand edited. Then the new set could be used for regression coefficient calculation and verification yielding meaningful RMS statistics.

D. Measurement of Equivalent Black-Body Temperature

The current technique for obtaining an equivalent black-body temperature from each AVHRR target analyzes the warm end of a histogram of the 121 AVHRR samples in each target. Using the truncated-normal technique, the uncontaminated mean of the clear samples is determined.

1. Truncated-Normal Assumptions

The truncated-normal technique assumes that clouds are colder than the surface temperature and that there are no surface temperature gradients. Erroneous retrievals are obtained under circumstances in which these assumptions are invalid.

2. Lack of Evaluation with Real Data

The behavior of the truncated-normal technique has not been studied at the raw data level with real sensor data. Perhaps the technique could be improved with tuning.

3. Need for Additional Cloud Information

It would be useful to have a count of the percentage of samples near the temperature of the retrieved black-body temperature. This count would allow an estimate of the amount of cloud contamination in the HIRS field of view.

E. Calibration Procedures

The AVHRR and HIRS/2 data are converted from counts to radiance using calibration coefficients given in the 1b data base. Conversion from radiance to temperature is performed by using the inverse of the Plank equation with a central wave number optimized for the range of temperatures expected for the ocean.

1. Use of Central Wave Numbers

Using a central wave number rather than the full information available in the spectral response curve results in errors up to 0.2^{0} C. As the accuracy of satellite-derived SST improves, it may be advantageous to do the calibration more precisely. Band corrections, not employed now, should be used with the HIRS/2 central wave numbers.

2. Inconsistency Between AVHRR and HIRS Window Channels

Differences between the HIRS and AVHRR window channels may be due to different spectral response or to cloud contamination. A third possibility is calibration differences. This should be investigated.

F. Field Analysis Procedures

Analyzed fields are created from satellite SST observations with a weighted-average objective analysis technique. A search circle is calculated about each gridpoint, and a weighted-average of all the observations occurring within the search circle is used to update the gridpoint. Those gridpoints having no data in the search circle retain the gridpoint temperature of the previous analysis. No relaxation to climatology is used.

1. Problems in Gulfs and Bays

In gulfs and bays where a portion of the bay is never more than 50 km from land, the SST field gridpoints in the bay or gulf still retain the initialization temperature inserted in November 1978. Erroneous contours are created in regions with inaccessible gridpoints (Figure 12). SST measurements of higher resolution and the use of the high resolution land/sea tags are necessary.

G. Minor Factors Affecting the Accuracy of Satellite SST

With the implementation of improvements reducing the effect of the factors discussed above, other error-producing factors will become relatively more important. These include:

1. Variation in the emissivity of water.

2. Attenuation of surface radiance by aerosols.

3. Temperature differences between the surface skin and the surface layer just beneath the skin (this results in an incompatibility of ship and satellite measurements).

4. Mislocation of the retrieved SST within a target (the temperature is always assigned to the center of the target rather than to the position within the target where the retrieved temperature actually occurs).

5. Lack of ice-edge information.

6. Diurnal variations in SST.

7. Differences between the point measurement of a ship or buoy and the area-integrated measurement of the satellite.